Barotropic Aspects of ITCZ Breakdown

ROSANA NIETO FERREIRA AND WAYNE H. SCHUBERT

Department of Atmospheric Science, Colorado State University, Fort Collins, Colorado

(Manuscript received 9 November 1995, in final form 21 June 1996)

ABSTRACT

In satellite images the ITCZ (intertropical convergence zone) is sometimes observed to undulate and break down into a series of tropical disturbances. Tropical cyclones may later develop within these disturbances and move into higher latitudes allowing the ITCZ to reform. It has been proposed that ITCZ breakdown results from a convectively modified form of combined barotropic and baroclinic instability of the mean flow. An unstable mean flow can be produced by ITCZ convection in just a couple of days. In this sense, the ITCZ produces favorable conditions for its own instability and breakdown.

In this study, a nonlinear shallow water model on the sphere is used to simulate barotropic aspects of ITCZ breakdown. In the shallow-water model, the ITCZ is simulated by a prescribed zonally elongated mass sink near the equator. The mass sink produces a cyclonic potential vorticity (PV) anomaly that has a reversed meridional PV gradient on its poleward side. According to the Ripa theorem, a flow that has a reversal in its meridional gradient of PV may become unstable in the presence of small disturbances. In the model simulations the unstable PV strip either undulates and breaks down into several cyclones or axisymmetrizes into one large cyclone.

The model results suggest that ITCZ breakdown may play a role in producing the observed tendencies for tropical storms to cluster in time and form poleward of the central latitude of the ITCZ and to the east of existing tropical storms. Additional experiments indicate that the observed higher frequency of tropical cyclogenesis just west of the Central American coast may be due to the horizontal morphology of the ITCZ in that region. In the eastern Pacific, the ITCZ is a zonally elongated line of convection that is climatologically wider on its eastern side. It is proposed that axisymmetrization of the PV strip produced by such an ITCZ is the cause of the increased frequency of tropical cyclogenesis just west of Central America.

Finally, the results obtained in this study point to the importance of zonal asymmetries inherent to the ITCZ in determining the flow evolution, suggesting the need for further studies of this effect. The importance of using forced simulations in the study of flow stability is also discussed.

1. Introduction

Climatologically, about 80% of all the tropical cyclones on the globe form near or within the ITCZ (intertropical convergence zone; Gray 1979). This motivates searching for mechanisms that favor tropical cyclogenesis within the context of ITCZ dynamics.

In satellite images, the ITCZ is sometimes observed to undulate, forming cloud patterns that resemble inverted Vs (Frank 1969). At times, such an undulating ITCZ breaks down into several tropical disturbances (Agee 1972; Thompson and Miller 1976) within which tropical cyclones may form, provided that favorable environmental conditions exist (Gray 1979; Zehr 1993). This process is referred to as ITCZ breakdown (Hack et al. 1989; Schubert et al. 1991; Guinn and Schubert 1993). The resulting tropical cyclones then move into higher latitudes, allowing the ITCZ to reform and perhaps start the cycle over again. A case of ITCZ breakdown that occurred in the east Pacific in July of 1988 is shown in Fig. 1. On 26 July (Fig. 1a), the ITCZ was an elongated zonal band of convection centered at about 10°N. Two days later, on 28 July (Fig. 1b), the ITCZ was undulating, giving rise to its breakdown into five tropical depressions by 30 July. Four of these depressions became tropical cyclones by 3 August (Fig. 1c; Gerrish and Mayfield 1989) and later moved into higher latitudes allowing the ITCZ to reform by 12 August (Fig. 1d). The undulations of the ITCZ seen in Fig. 1 are the signature of easterly waves in the tropical troposphere.

Riehl (1945) was among the first to recognize the existence of easterly waves and their importance in tropical cyclogenesis. Easterly waves have since been observed in the Atlantic Ocean and West Africa (Carlson 1969; Burpee 1972, 1975; Reed et al. 1977; Chen and Ogura 1982), in the Pacific Ocean (Yanai 1961; Reed and Recker 1971; Chang 1970; Nitta et al. 1985; Tai

Corresponding author address: Dr. Rosana Nieto Ferreira, Department of Atmospheric Science, Colorado State University, Fort Collins, CO 80523.
E-mail: rosana@bjerknes.atmos.colostate.edu

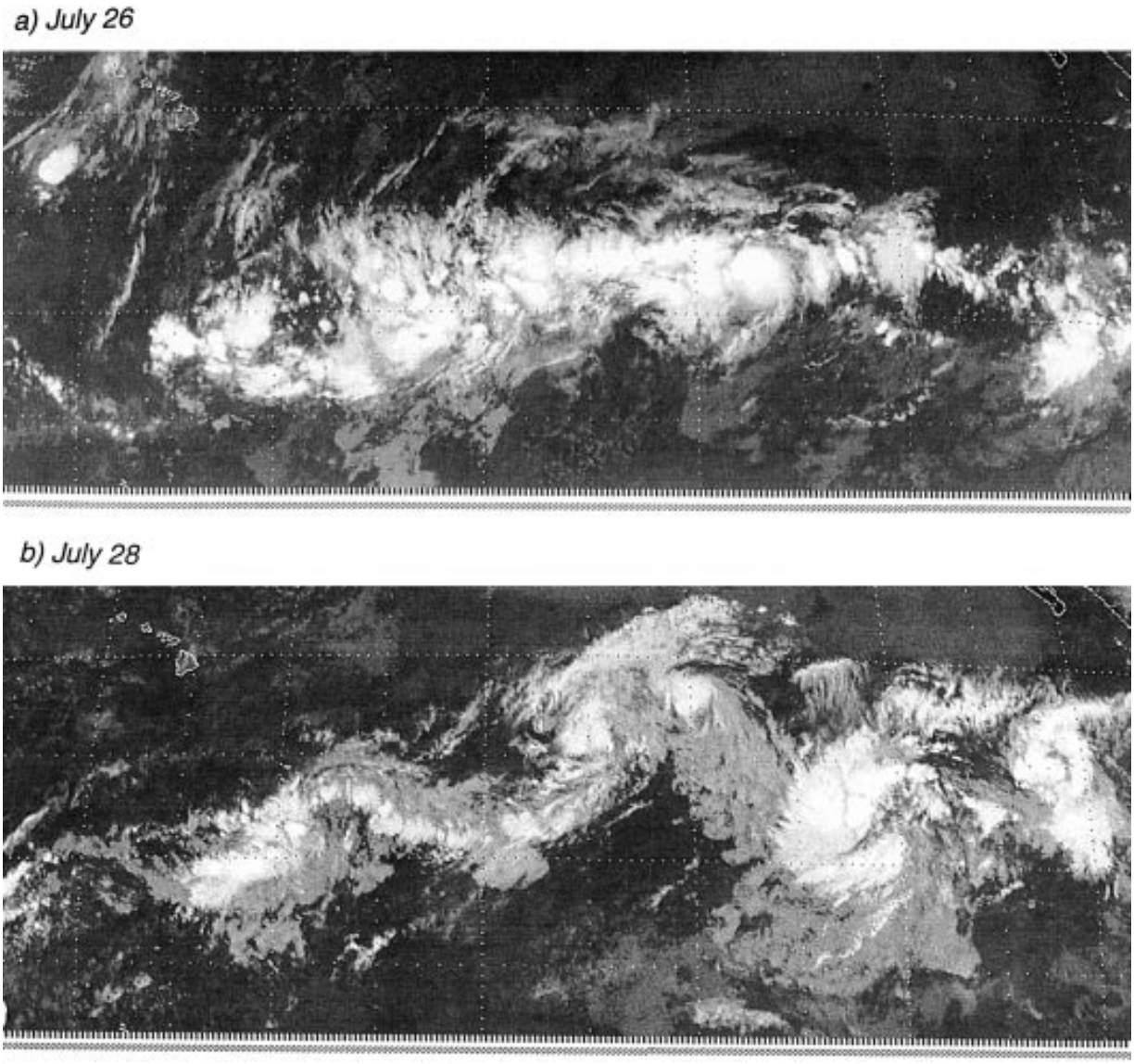

FIG. 1. GOES IR images at 1646 UTC on (a) 26 July, (b) 28 July, (c) 3 August, and (d) 12 August 1988 showing a case of ITCZ breakdown. The images cover a region of the eastern Pacific between 2°N and 24°N, 108°W and 165°W. Hawaii is at the upper left and Baja California at the upper right corners of the images.

and Ogura 1987; Heta 1991), and in the South China Sea and India (Saha et al. 1981). These studies have found that easterly waves occur in the lower tropical troposphere and have typical wavelengths and speeds that range from 2000 to 4000 km and 5 to 8 m s^{-1}, respectively.

Nearly 60% of all Atlantic tropical cyclones originate from African easterly waves (e.g., Avila and Clark 1989). Observational (Burpee 1972; Norquist et al. 1977) and numerical (see Thorncroft and Hoskins 1994a,b for a comprehensive review) studies indicate that African easterly waves result from a convectively modified form of combined barotropic and baroclinic instability of the African easterly jet.[1] The relative importance of barotropic and baroclinic processes in the formation of African easterly waves is not yet well established. For instance, observations suggest that African easterly waves are primarily maintained by barotropic energy conversions over the Atlantic Ocean, west of 15°W (Norquist et al. 1977; Thompson et al. 1979) and baroclinic energy conversions over Africa (Norquist et al. 1977; Burpee 1972). Linear numerical

[1] The African easterly jet has maximum winds of 10–15 m s^{-1} near 700 mb and 15°N.

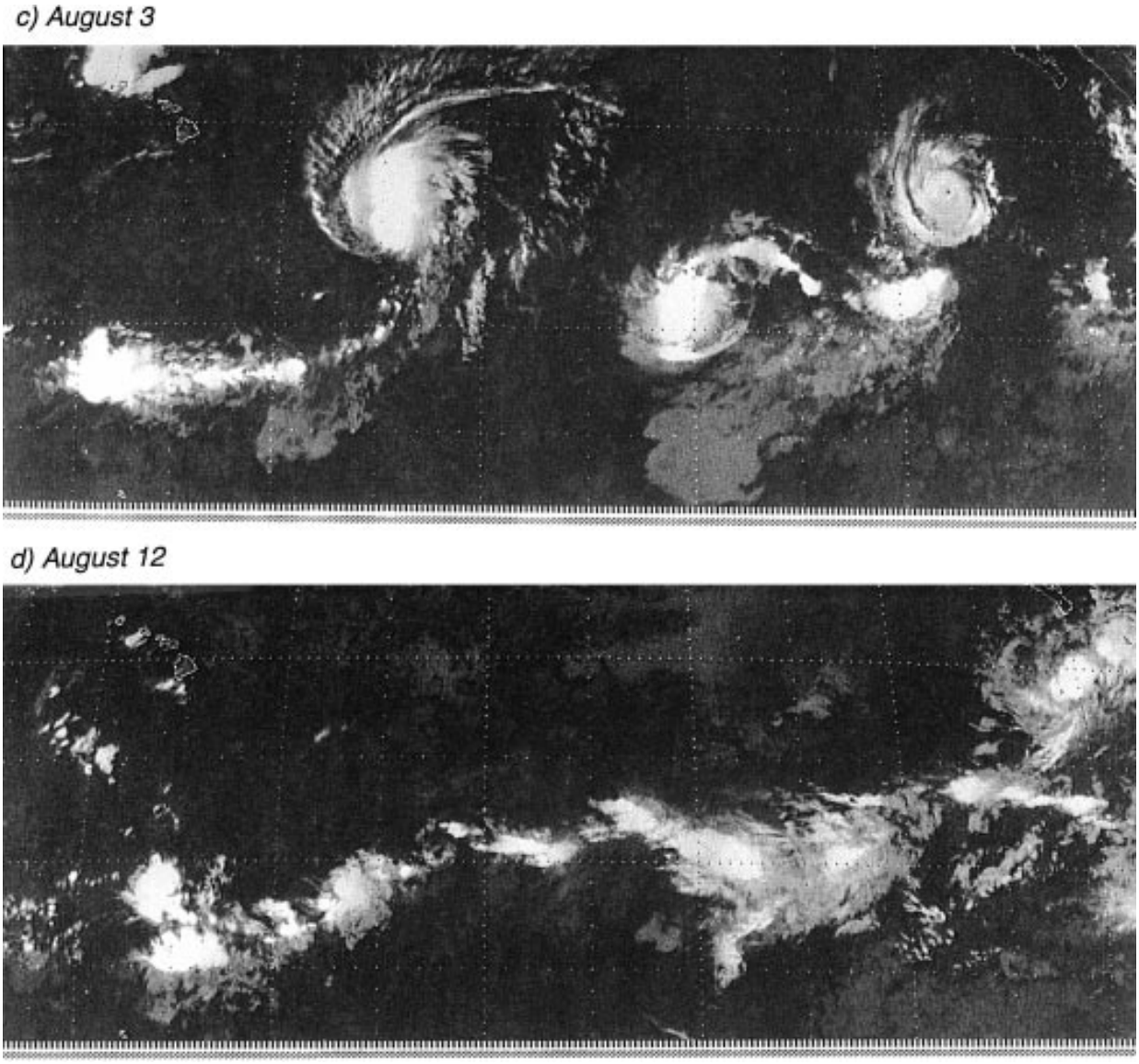

FIG. 1. (*Continued*)

studies of the stability of the African easterly jet concluded that barotropic conversions are the dominant source of energy for the most unstable waves (e.g., Thorncroft and Hoskins 1994a). On the other hand, a nonlinear study by Thorncroft and Hoskins (1994b) shows that the growth of African easterly waves is dominated by barotropic energy conversions during the first week and by baroclinic energy conversions thereafter.

The existence of the African easterly jet is possibly due to the combined effects of ITCZ convection (Schubert et al. 1991) and thermal wind balance over the strong surface meridional temperature gradient between the warm Saharan air and the colder air over the Guinea Gulf (Burpee 1972).[2] However, in the oceanic regions where easterly waves are observed, the lack of strong underlying meridional temperature gradients implies that ITCZ convection should be the dominant effect in producing the unstable flow in which the waves form, unless they can be shown to have propagated from Africa. That is the case in the Atlantic Ocean and Caribbean Sea where the majority of easterly waves have

[2] The location of the African easterly jet coincides with the strongest meridional temperature gradient at the surface, which is displaced northward of the coastline because of the influence of the monsoonal southwesterlies in the African bulge.

African origin. In the eastern Pacific, easterly waves may either form in situ (Nitta et al. 1985; Tai and Ogura 1987) or propagate from the Atlantic basin (e.g., Avila and Clark 1989). In the western Pacific, on the other hand, easterly waves form locally in the low-level mean unstable flow that exists during the summer months (Nitta and Yanai 1969; Nitta and Takayabu 1985).

In ITCZ breakdown, the unstable flow is produced by latent heat release in deep cumulus convection within the ITCZ. In the lower troposphere, ITCZ convection produces a cyclonic potential vorticity (PV) anomaly that has a reversal of the meridional PV gradient on its poleward side and therefore satisfies the necessary condition for combined barotropic and baroclinic instability[3] (Charney and Stern 1962). The ITCZ may then start undulating due to combined barotropic and baroclinic instability and finally break down into a series of tropical disturbances. The subsequent formation of tropical cyclones within these tropical disturbances is contingent on the existence of favorable environmental conditions. These tropical cyclones later move into higher latitudes allowing the ITCZ to reform.

Guinn and Schubert (1993) used a shallow-water model on an f plane to show that elongated strips of cyclonic PV undulate and break down into cyclones in a way that resembles the break down of the ITCZ observed in nature (Fig. 1). Given the importance of barotropic instability in ITCZ breakdown (e.g., Thorncroft et al. 1994a,b), a global nonlinear shallow-water model is used in this study to investigate barotropic aspects of the formation of tropical disturbances through ITCZ breakdown. This paper is organized as follows. Section 2 introduces the shallow-water model. The numerical aspects of the model are presented in appendix A. In section 3, initial value experiments showing the nonlinear breakdown of zonally symmetric PV strips on the sphere are presented. The interaction of a zonally symmetric PV strip and a nearby cyclone[4] is also studied in initial value experiments discussed in section 4. Sections 5 and 6 show simulations with localized zonally elongated mass sinks that study how zonal asymmetries in the ITCZ affect the formation of tropical disturbances. Finally, a summary of the model results and related conclusions are presented in section 8.

2. The shallow-water equations

A nonlinear spectral shallow-water model on the sphere will be used in sections 3–6 to study ITCZ breakdown. The shallow-water model is a useful simple tool to study tropical atmospheric phenomena that are dominated by horizontal advection of PV and barotropic instability. The shallow-water equations are

$$\frac{\partial u}{\partial t} - \zeta v + \frac{\partial\left[gh + \frac{1}{2}(u^2 + v^2)\right]}{a\cos\phi\partial\lambda} = 0, \tag{1}$$

$$\frac{\partial v}{\partial t} + \zeta u + \frac{\partial\left[gh + \frac{1}{2}(u^2 + v^2)\right]}{a\partial\phi} = 0, \tag{2}$$

$$\frac{\partial h}{\partial t} + \frac{\partial(hu)}{a\cos\phi\partial\lambda} + \frac{\partial(hv\cos\phi)}{a\cos\phi\partial\phi} = Q, \tag{3}$$

where

$$\zeta = 2\Omega\sin\phi + \frac{\partial v}{a\cos\phi\partial\lambda} - \frac{\partial(u\cos\phi)}{a\cos\phi\partial\phi} \tag{4}$$

is the absolute vorticity. Here u and v are the zonal and meridional components of velocity; h is the fluid depth; a is the radius of the earth; λ and ϕ are longitude and latitude, respectively; and Q is a mass sink or source. Equations (1)–(3) form a closed system in u, v, and h. The numerical method used in the model integration is based on spherical harmonics and is outlined in appendix A. Spectral blocking is controlled by adding hyperdiffusion terms to Eqs. (1)–(3), as discussed in appendix A. Triangular truncation with a maximum total wavenumber $N = 213$ is used in the simulations shown in this study. With a T213 truncation the number of real degrees of freedom for each dependent variable is $(213)^2$. If an equal area of the surface of the earth is associated with each real degree of freedom, this area equals $4\pi a^2/(213)^2 \approx 11\,239$ km^2. The square root of this area, which turns out to be approximately 106 km, is a useful estimate of the horizontal resolution of the T213 spherical harmonic spectral model (for further discussion, see Laprise 1992).

Equations (1)–(3) can be combined to yield the potential vorticity conservation principle

$$\frac{DP}{Dt} = -\frac{PQ}{h}, \tag{5}$$

where the material derivative is given by

$$\frac{D}{Dt} = \frac{\partial}{\partial t} + u\frac{\partial}{a\cos\phi\partial\lambda} + v\frac{\partial}{a\partial\phi} \tag{6}$$

and the potential vorticity by

$$P = \left(\frac{\bar{h}}{h}\right)\zeta, \tag{7}$$

with the constant mean initial fluid depth $\bar{h}$ introduced so that the potential vorticity, P, has the same units as the absolute vorticity, ζ.

[3] An analogous mechanism has been proposed for the formation of frontal waves in the midlatitudes. Joly and Thorpe (1990) proposed that latent heat released by convection in regions of strong frontogenesis produces a lower-tropospheric elongated zone of high PV along the front. Their model results showed that, as frontogenesis weakens, frontal waves are produced due mainly to barotropic instability of the elongated PV strip.

[4] The term *cyclone* is hereafter used to designate closed cyclonic circulations.

The damping rates introduced by hyperdiffusion are small enough (see appendix A) that it is probably useful to view the flow simulations as essentially conservative except for the mass source or sink term (Q) in Eq. (5). Note that although the domain of the model is the entire sphere, only a portion of it is shown for all simulations.

3. Breakdown of zonally symmetric PV strips

In this section, the shallow-water model is used to study the breakdown of an idealized zonally symmetric ITCZ. The lower-tropospheric flow around this idealized ITCZ is described by a zonally symmetric vorticity strip given by

$$\zeta(\lambda, \phi, 0) = \begin{cases} 2\Omega \sin \phi + \xi_s & \text{for } |\phi - \phi_c| \le \phi_w/2 \\ 2\Omega \sin \phi & \text{otherwise,} \end{cases} \quad (8)$$

where ϕ_c, ϕ_w, and ξ_s are the central latitude, width, and magnitude of the vorticity strip, respectively. In the shallow-water simulation, the parameters $\phi_c = 10°$N, $\phi_w = 4.5°$, and $\xi_s = 3.0 \times 10^{-5}$ s^{-1} were chosen to approximate the average summer latitude of the ITCZ in the North Pacific Ocean (e.g., Waliser and Gautier 1993) and to produce a shear layer that is comparable in width and strength to that produced in the forced experiment discussed in section 5. The meridional absolute vorticity profile is given by the solid line in Fig. 2. The wind field associated with this vorticity strip consists of a 4.5° wide shear layer that has a 15 m s^{-1} shear between the easterlies to its north and westerlies to its south. The mean initial fluid depth $\bar{h}$ was set to 222 m, which implies a gravity wave phase speed of 46.6 m s^{-1} and an equatorial Rossby length $[a(g\bar{h})^{1/2}/(2\Omega)]^{1/2}$of 1440 km. This fluid depth is chosen because the tropical tropospheric response to organized convection is dominated by baroclinic modes whose equivalent fluid depths range between 100 and 500 m (e.g., Fulton and Schubert 1985). Nonlinear balance (appendix A) was initially assumed to obtain the mass fields.

The meridional gradient of absolute vorticity is reversed on the northern edge of the aforementioned vorticity strip (solid line in Fig. 2) implying that Rayleigh's necessary condition for barotropic instability of a nondivergent flow is satisfied. A nondivergent, multiregion linear normal mode stability analysis of the vorticity strip (following Dritschel and Polvani 1992) determined that its most unstable mode has zonal wavenumber 13, westward phase speed of $\sim$ 1.6 m s^{-1}, and e-folding time of 2 days. In agreement with previous studies of barotropic instability (e.g., Kuo 1973; Joly and Thorpe 1990), the wavelength of the most unstable mode ($\sim$ 3000 km) is about 12 times the half-width of the PV strip.

At the begining of the simulation, the PV strip is perturbed with a wavenumber 13 disturbance that has an amplitude of 10^{-7} s^{-1}. This means that the initial fluid depth, wind, and PV fields are nearly zonally symmetric. As the initial disturbance grows by extracting energy from the mean flow through the barotropic instability process, the cyclonic PV strip and corresponding mass and wind fields undulate (Fig. 3a). During breakdown, the high PV in the strip becomes pooled into cyclones that are connected by thin PV filaments. These cyclones are initially zonally elongated (Fig. 3b) and as breakdown proceeds, they tend to axisymmetrize (Fig. 3c). Meanwhile, the PV filaments become thinner and longer and wrap around the cyclones. Axisymmetrization is a nonlinear process in which PV is stripped out of the cyclone core forming the PV filaments (e.g., Melander et al. 1987). Strain and adverse shear created by the cyclones prevent the PV filaments from further breakdown due to barotropic instability (e.g., Dritschel 1989; Dritschel et al. 1991). As proposed by Guinn and Schubert (1993), the high PV filaments that form during ITCZ breakdown may be the outer spiral bands of hurricanes (e.g., Fig. 1c). At 15 days (Fig. 3c) the filaments

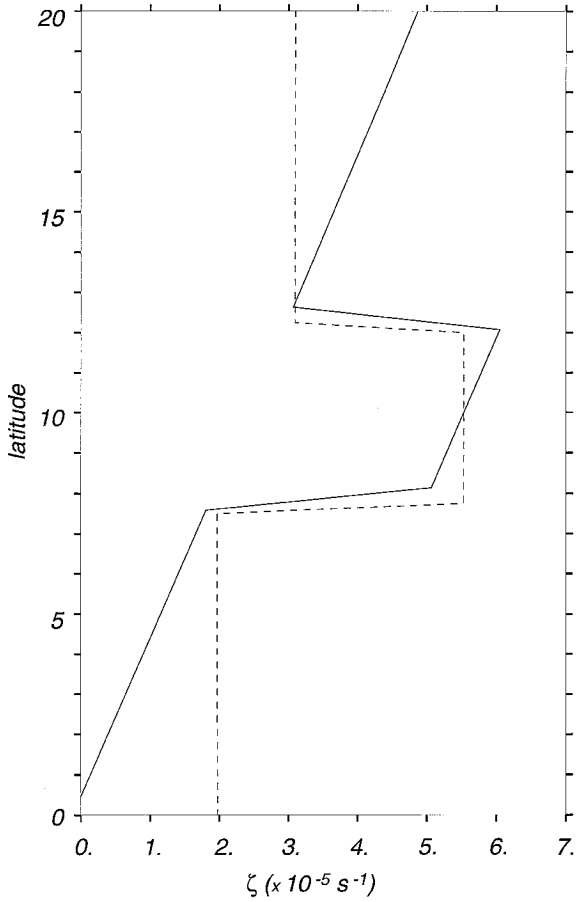

FIG. 2. Meridional profiles of absolute vorticity. The solid line shows the meridional profile of absolute vorticity given by Eq. (8) with $\phi_c = 10°$N, $\phi_w = 4.5°$, and $\xi_s = 3.0 \times 10^{-5}$ s^{-1}. The dashed line is the approximation to the vorticity strip given by the solid line that is studied using the three-region model discussed in appendix B.

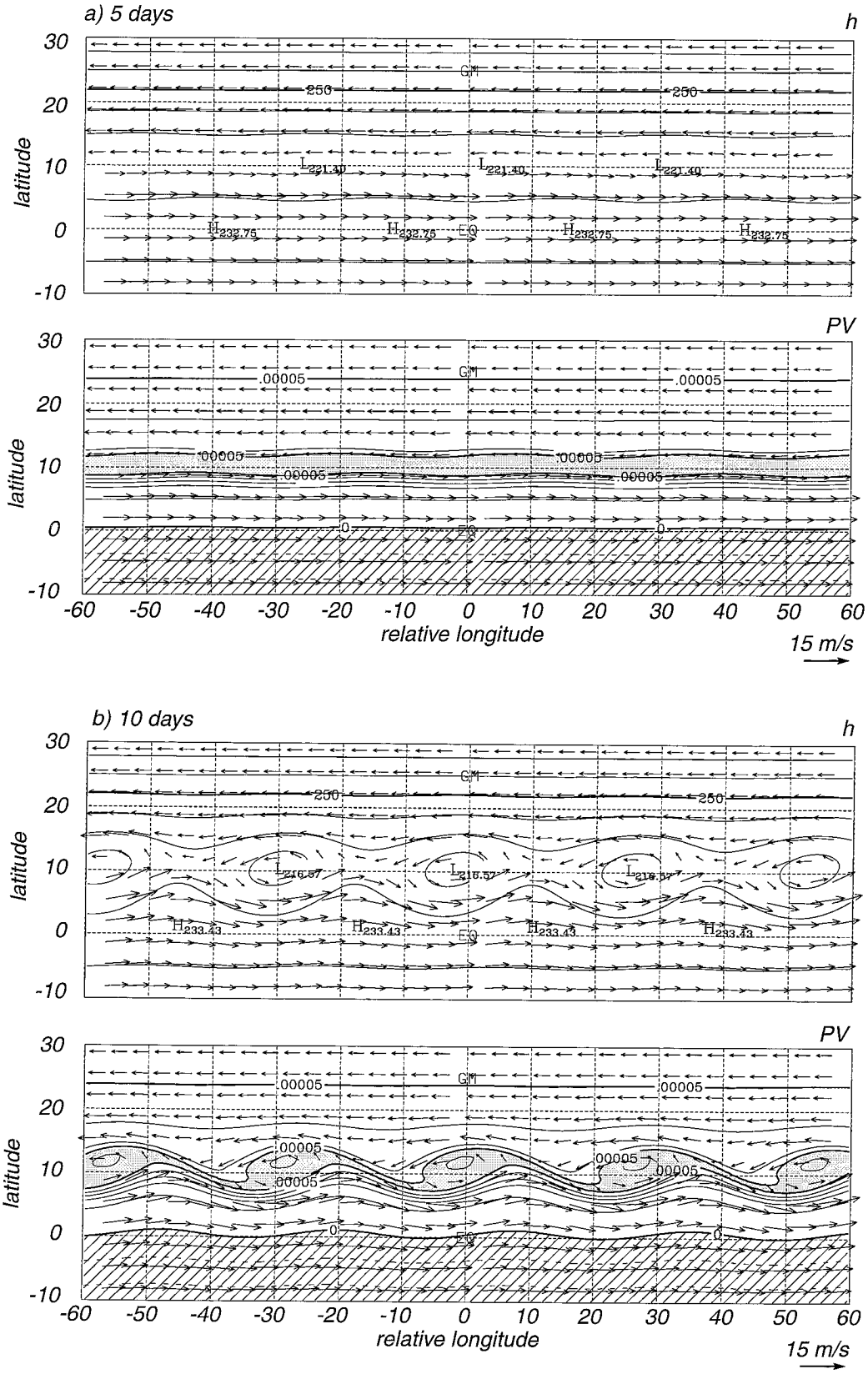

FIG. 3. Breakdown of a 4.5° wide zonally symmetric vorticity strip centered at 10°N with maximum relative vorticity 3.0×10^{-5} s^{-1}. The displayed fields are fluid depth (m), PV (s^{-1}), and winds (m s^{-1}) at (a) 5 days, (b) 10 days, and (c) 15 days.

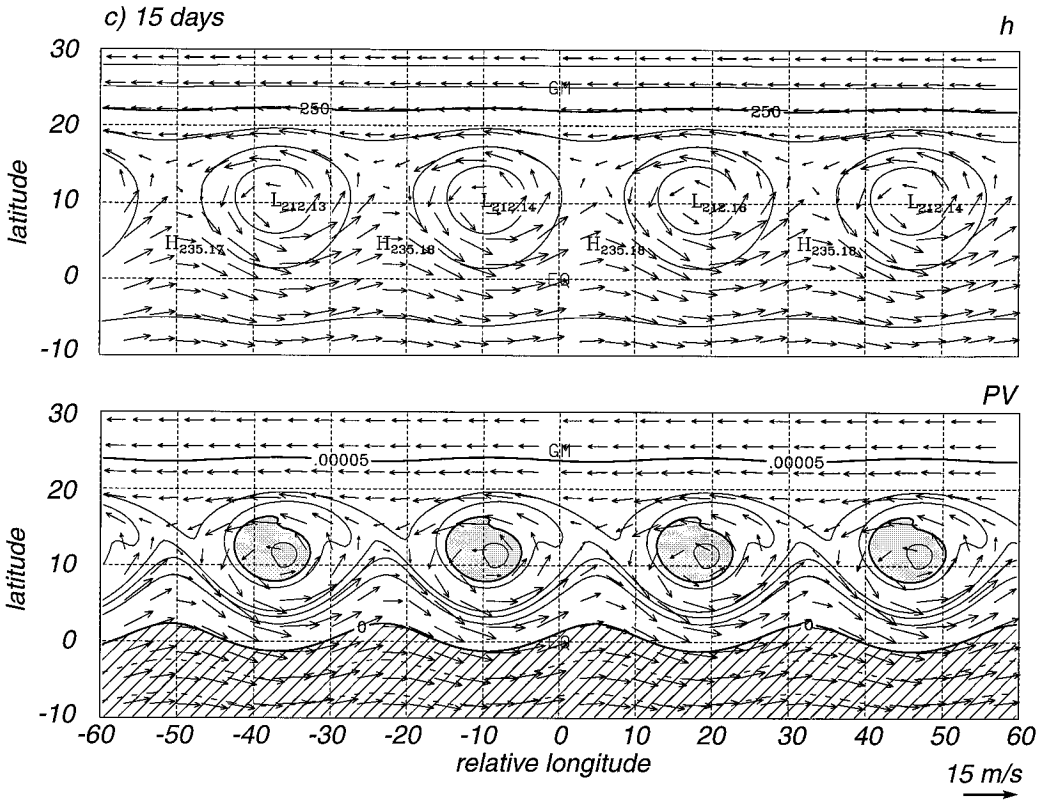

FIG. 3. (*Continued*)

of high PV that linked the cyclones have been detached due to model dissipation, which is strongest in the smaller scales. Throughout the simulation, the cyclones propagate westward at about 1.8 m s^{-1}, in good agreement with the linear normal mode analysis calculation.

An interesting feature in Fig. 3c is that the amplitude of the wave in the westerlies (to the south of the PV anomaly) is larger than the amplitude of the wave in the easterlies (to the north of the PV anomaly). This asymmetry is an effect of the planetary vorticity gradient, which causes the isolines of PV to be more closely packed on the southern than on the northern side of the PV strip (Fig. 3a). In other words, the absolute value of the meridional PV gradient is larger on the southern than on the northern edge of the PV strip. In order to understand the ensuing asymmetry in flow waviness between the northern and southern sides of the PV strip, it is useful to approximate the vorticity profile given by the solid line in Fig. 2 by the three-region profile given by the dashed line in Fig. 2. This simplified vorticity strip shares some important attributes with the original one, namely that its crosswise wind shear is nearly the same, the absolute value of the jump in vorticity is larger on its southern than on its northern side, and there is a reversal in the meridional vorticity gradient on its northern edge. The latter feature implies that counterpropagating vorticity waves are possible. The streamfunctions associated with the most unstable mode for the simplified vorticity strip (obtained using the method outlined in appendix B) are shown in Fig. 4. Note how the amplitude of the vorticity wave on the southern edge of the vorticity strip (Ψ_s; Fig. 4c) is larger than that of the wave on the northern edge of the vorticity strip (Ψ_n; Fig. 4b). The total solution, Ψ (Fig. 4a), is a superposition of Ψ_s and Ψ_n (Fig. 4b). The wave on the reversed meridional PV gradient on the poleward edge of the strip (Ψ_n) propagates eastward relative to the zonal flow and the wave on the positive meridional PV gradient on the equatorward edge of the strip (Ψ_s) propagates westward relative to the zonal flow. On the poleward edge of the PV strip, easterly flow opposes the relative eastward propagation of the vorticity wave. Likewise, on the equatorward edge of the PV strip westerly flow opposes the relative westward propagation of the vorticity wave. In this case, the counterpropagating waves phase lock and amplify (Hoskins et al. 1985), a result closely connected with the Fjørtoft necessary condition for instability of nondivergent, barotropic flow[5] (Drazin and Reid 1981).

[5] Of course, the numerical simulations presented here use the divergent barotropic model so the above nondivergent Rayleigh and Fjørtoft theorems are not strictly applicable. However, if the more general divergent barotropic stability results of Ripa (1983) are used, the conclusions concerning the possible instability of the above flow are unchanged.

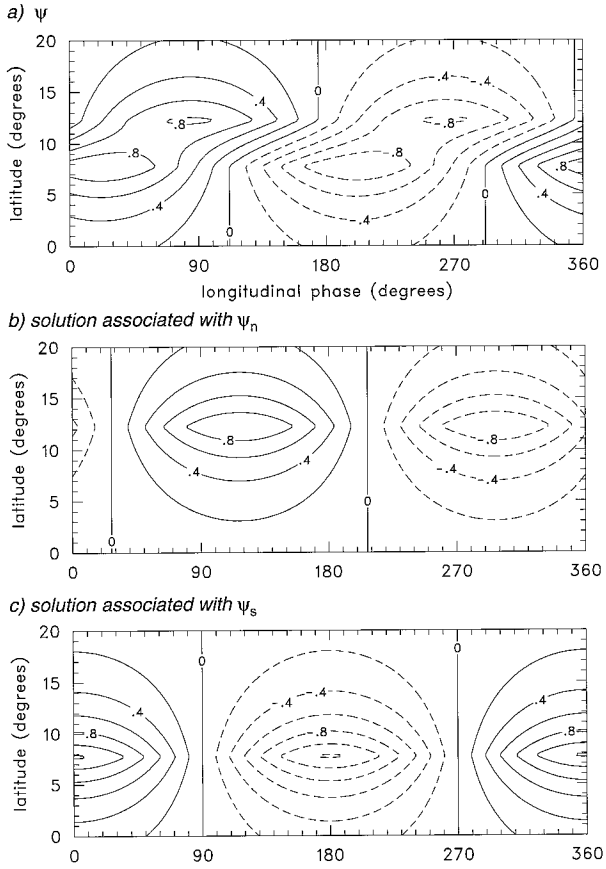

FIG. 4. Streamfunction of the most unstable mode calculated for the simplified vorticity strip given by the dashed line in Fig. 2: (a) total streamfunction solution determined from (B5), (b) solution associated with Ψ_n, and (c) solution associated with Ψ_s. All fields are normalized by the maximum streamfunction value. Note that the streamfunction solution has a larger amplitude on the equatorward side of the PV strip.

In the simplified three-region model, the asymmetry in the amplitude of the waves on the northern (Ψ_n) and southern (Ψ_s) sides of the vorticity strip reflects the asymmetry in the jumps of absolute vorticity between the northern and southern sides of the strip. Likewise, the larger amplitude of the wave on the equatorward side of the PV strip in Fig. 2c reflects the fact that the absolute value of the meridional PV gradient is larger to the south than to the north of the PV strip. Some evidence that this asymmetry occurs in observed easterly waves can be found in Fig. 2 of Takayabu and Nitta (1993) and Fig. 16 of Numaguti et al. (1995).

In the regions where there is exchange of mass between the two hemispheres with intrusion of negative PV air from the Southern into the Northern Hemisphere and vice versa (Fig. 2c), $fP < 0$, and the necessary condition for occurrence of inertial instability is met. However, since inertially unstable modes have very slow growth rates for flows with large $\bar{h}$ (Stevens 1983), they are not apparent in any of the simulations shown here.

Additional simulations were performed (not shown) to study the effects of changing the width and intensity of the PV strip. In agreement with linear normal mode stability analysis, the width and intensity of the PV strip are directly proportional to the scale of the most unstable mode and the rate of breakdown, respectively. In addition, the characteristics of the most unstable modes in such relatively thin PV strips change very little with changes in latitude within about 30° from the equator.

4. Interaction between a cyclone and a zonally symmetric PV strip

An interesting example of interaction between the ITCZ and a nearby tropical cyclone occurred in the east Pacific Ocean in July 1978 (Fig. 5). After its formation near 13.6°N, 111.4°W on 10 July, Hurricane Fico followed a long westward trajectory at an average speed of about 5.3 m s^{-1} until 21 July when it recurved and moved into higher latitudes (Gunther 1979). The circulation of the hurricane produced a perturbation on the ITCZ that accompanied the storm in its westward movement until it recurved on 21 July. As the hurricane moved into higher latitudes, its influence on the ITCZ decreased.

An idealized barotropic counterpart of this process is obtained when the model is initialized with a zonally symmetric cyclonic PV strip and a cyclone nearby. The radial distributions of relative vorticity and nondivergent tangential wind for a cyclone centered at 15°N with a relative vorticity of 2.0×10^{-4} s^{-1} and 2° in radius are shown in Fig. 6. The outer core wind distribution of this cyclone falls within the observed range of outer core tangential winds of tropical cyclones (Merrill 1984). A higher spatial resolution would be needed to obtain a good representation of the inner core winds. However, it is expected that the interaction of the idealized cyclone with the PV strip should be more dependent on the outer core winds than on the intensity of the storm, just as is the case for tropical cyclone motion (e.g., Chan and Williams 1987).

A reference simulation with a cyclone initially at 15°N in a quiescent flow is shown in Fig. 7. After 10 days (Fig. 7a) the cyclone has drifted to 29°N and the dispersion of short Rossby wave energy has produced a wave train to the southeast of the cyclone (Hoskins et al. 1977). Approximately 1500 km southeast of the hurricane is a cyclonic region that is the largest amplitude part of the Rossby wave train extending southeastward. On the east edge of this particular cyclonic region, the flow is parallel to the PV contours and on the west edge, the flow is across the PV contours in the sense of producing a broadening trough (Thorncroft et al. 1993). This broadening trough is about to enter the highly nonlinear phase of a ''cyclonic breaker'' that involves the wrap-up of PV contours. After 15 days (Fig.

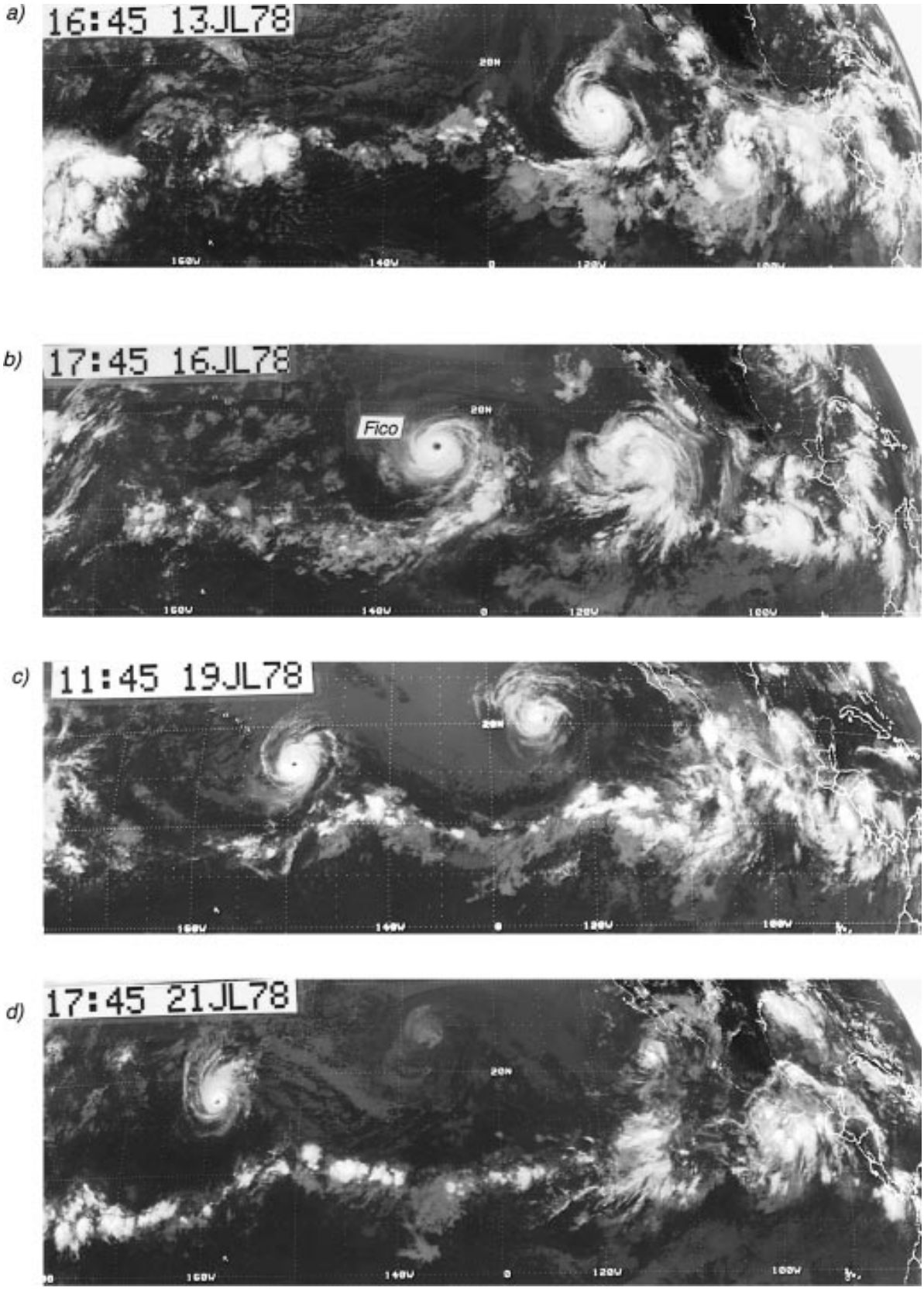

FIG. 5. GOES infrared satellite images for the east Pacific during the period between 13 and 21 July 1978 (time is UTC). The sequence illustrates the interaction of Hurricane Fico with the ITCZ.

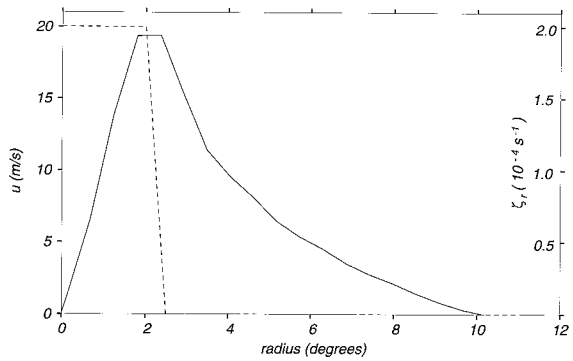

FIG. 6. Radial profiles of relative vorticity (dotted line) and tangential wind (solid line) distributions for a 2°-radius cyclone with $\zeta_v = 2.0 \times 10^{-4}$ s^{-1} and $\phi_c = 15$°N.

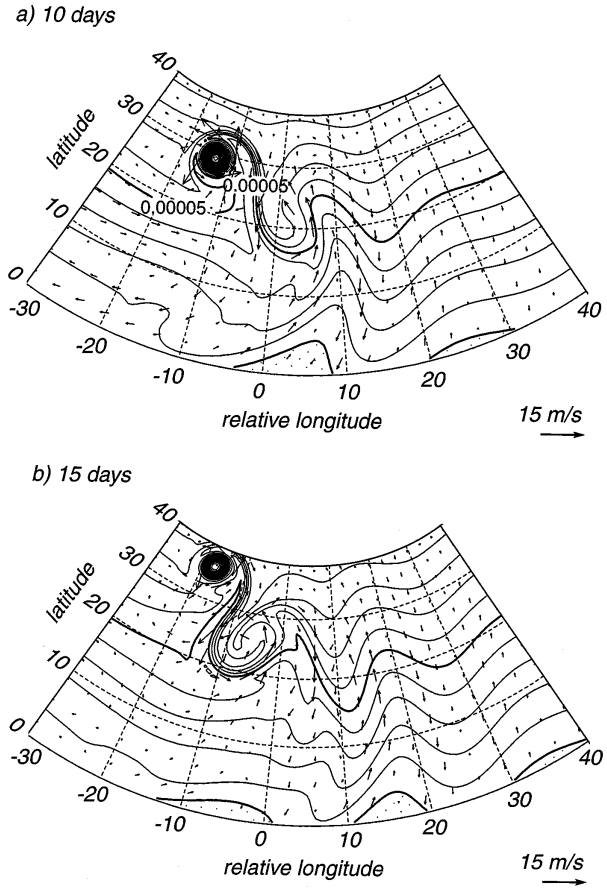

FIG. 7. Evolution of PV (s^{-1}) and winds (m s^{-1}) for a 2° radius cyclone with $\zeta_v = 2.0 \times 10^{-4}$ s^{-1} and $\phi_c = 15$°N that was initially in a quiescent environment: (a) at 10 days and (b) at 15 days.

7b), a secondary cyclone has been produced just to the southeast of the original cyclone with half its intensity. A third cyclonic region farther southeast of the original cyclone has also begun the nonlinear phase of its evolution.

The interaction of the cyclone with a 4.5° wide zonally symmetric PV strip centered at 10°N with a relative vorticity of 3×10^{-5} s^{-1} is shown in Fig. 8. The initial wind and fluid depth fields are in nonlinear balance. In order to avoid negative fluid depths in and near the cyclone, the mean initial fluid depth was increased to 4500 m, which implies a gravity wave phase speed of 210 m s^{-1} and an equatorial Rossby length of 3000 km. The necessary criterion for barotropic instability is again met just to the north of the PV strip. By day 2 (Fig. 8a), the cyclone has begun to wrap the PV strip around itself. To the east of the cyclone, dispersion of short Rossby wave energy produces undulations in the PV strip whose amplitude decreases with increasing distance from the cyclone. Comparison of Figs. 7a and 8c shows that the presence of the zonally symmetric PV strip to the south of the cyclone has the effect of reducing the intensity of short Rossby wave energy dispersion.[6] As the simulation advances, the undulations amplify (Fig. 8b) through barotropic instability, causing that portion of the PV strip to break down into several cyclones (Fig. 8c). The wavenumber of the most unstable mode selected for this PV strip is the same in the experiments shown in this section and in section 3. Hence, the wavelength of the most unstable mode does not depend on the type of perturbation imposed as should be expected from linear stability results.

Throughout the simulation, the cyclone continuously moves west-northwestward at an average speed of 8 m s^{-1} (trajectory A in Fig. 9). The initial perturbation on the PV strip just to the southeast of the cyclone follows the westward movement of the cyclone at a somewhat slower speed. By the end of the simulation, the cyclone has increased in size and its influence on the PV strip has decreased as a consequence of the northward displacement of the cyclone with respect to the PV strip. This evolution qualitatively resembles the interaction between Hurricane Fico and the ITCZ shown in the satellite image sequence in Fig. 5.

Figure 9 shows the trajectories followed by the cyclone under the influence of the zonally symmetric PV strip (A) and in a quiescent environment (B). The poleward and westward trajectory followed by a cyclone in a quiescent environment (B) is solely dictated by β drift, which consists of linear and nonlinear interactions between the circulation of the cyclone and the meridionally varying planetary vorticity (e.g., Li and Wang 1994). In the presence of a cyclonic PV strip to its south, the trajectory of the cyclone becomes longer and more zonal. The PV strip affects the movement of the cyclone mainly through the advection by its steering flow, which is easterly to the north of the PV strip, but also through the change in the environmental meridional vorticity

[6] The intensity of short Rossby wave dispersion is also reduced by a reduction of the initial cyclone's relative angular momentum (Shapiro and Ooyama 1990).

gradient it introduces. The meridional gradient of relative vorticity acts to oppose β drift when its sign is opposite to the planetary vorticity gradient and to enhance it when they are of the same sign (Evans et al. 1991).

In the Pacific Ocean, tropical cyclones are nearly twice as likely to form to the east of existing tropical cyclones than to their west (Frank 1982). The simulations presented in this section suggest that this trend may be due to short Rossby wave dispersion by either producing a strong trough just to the east of the existing tropical cyclone (Holland 1995) or initiating breakdown of a nearby ITCZ. However, the tendency for formation of new storms to the east of existing ones may also simply be an artifact of the westward movement of the cyclones away from their preferred regions of origin.

5. The breakdown of an ITCZ of limited zonal extent

In the previous two sections, the ITCZ was idealized as a zonally symmetric cyclonic PV strip circling the sphere near the equator. However, at any individual time the ITCZ is not zonally symmetric, but a rather discontinuous zonal band of convection of varying width. In this section, forced simulations are used to study the effect of zonal asymmetries upon the breakdown of the ITCZ.

A more realistic representation of the transient and zonally asymmetric ITCZ is in the form of a localized, zonally elongated mass sink near the equator. According to Eq. (5), an imposed mass sink produces a positive PV anomaly in the Northern Hemisphere in a way that is analogous to the effect of convection on the lower troposphere (e.g., Schubert et al. 1991). The mass sinks used in this study are highly idealized proxies for the ITCZ. For instance, they do not represent the transient smaller scales of convection that are embedded in the ITCZ and would produce finer-scale features in the PV fields. However, the smoothing associated with the inversion of the elliptic operator in Eq. (A.9) renders the flow and mass fields nearly insensitive to the details of the PV field.

Results obtained in simulations with mass sinks of various dimensions and locations are discussed in this section. The spatial and temporal variations of the mass sink are given by

$$Q(\lambda, \phi, t) = Q_0 \mathcal{F}[r(\lambda, \phi), 30] \mathcal{F}[\tau(t), 320], \quad (9)$$

where

$$\mathcal{F}(x, \gamma) = \begin{cases} 1 - \exp\left[-\dfrac{\gamma}{x}\exp\left(\dfrac{1}{x-1}\right)\right], & \text{for } 0 < x < 1 \\ 0, & \text{otherwise} \end{cases} \quad (10)$$

is a smooth unit step function, with

$$r(\lambda, \phi) = [(\lambda \cos \phi)^2/b^2 + (\phi - \phi_0)^2/(c\sigma)^2]^{1/2}$$

and $\tau(t) = |2t/t_0 - 1|$. The constants ϕ_0, b, c, t_0, Q_0 determine the latitude where the forcing is centered, its zonal and meridional extent, duration, and magnitude, respectively. The parameter σ is used to deform the shape of the ellipse. For the integrations shown in this section, the model begins from a state of rest with a constant fluid depth of 222 m. The dimensions of the mass sink were chosen to approximate the ITCZ configuration shown in Fig. 1. The specified constants are $\phi_0 = \pi/18$ (10°N), $\sigma = 1$ (perfect ellipse), $b = \pi/3$, and $c = \pi/36$. The nondimensional steepness parameters ($\gamma = 30$ for space and $\gamma = 320$ for time) determine the spatial and temporal scales over which the unit step is smoothed. Figure 10 summarizes the spatial and temporal structures of the mass sink. The mass sink was applied for 5 days ($t_0 = 5$ days) in order to produce a shear layer with easterlies of ~ 5.5 m s^{-1} and westerlies of ~ 12 m s^{-1}. Although such high shears are not observed in climatologies of lower-level tropical flows, it is possible that they are observed in daily maps. Such shears are, however, produced by zonally symmetric, stratified Hadley cell models (e.g., Hack et al. 1989) in just a few days of convection having an apparent heat source typical of tropical convection. In the shallow-water model, a reasonable timescale for the flow evolution occurs when the value $Q_0 = -55.2$ m day^{-1} is chosen in agreement with Fulton and Schubert's (1985, their Table 5) vertical normal mode projections of ITCZ apparent heat source profiles. During its 5 days of activity this mass sink produces a one percent decrease in the initial globally integrated mass.

Figure 11 shows the temporal evolution produced by the zonally elongated mass sink described above. A reversal in the PV gradient first appears during day 2 of the integration, providing the necessary condition for the occurrence of barotropic instability. This is in agreement with the conclusion in Hack et al. (1989) that only a couple of days of convection are needed to produce a reversal in the meridional PV gradient. Figure 11a shows the results at 5 days, when the mass sink has just been turned off. The cyclonic PV anomaly is most intense in the poleward half of the mass sink and has slightly rotated cyclonically around its center due to self-advection. In the f plane, Guinn and Schubert (1993) show a PV strip that rotates nearly 60° around its axis by the time it breaks down into two cyclones. Here, the presence of a meridionally varying planetary vorticity inhibits rotation, and the PV strip seems to find an equilibrium inclination with respect to the equator. Additional simulations show that the longer the PV strip, the smaller its tilt with respect to the equator. By day 8 (Fig. 11b), the PV strip has begun undulating in a wavenumber 19 (or a wavelength of about 2070 km) pattern, and two zonally elongated cyclones are emerging on its westernmost portion. After 11 days (Fig. 11c), the PV strip has broken down into three cyclones linked

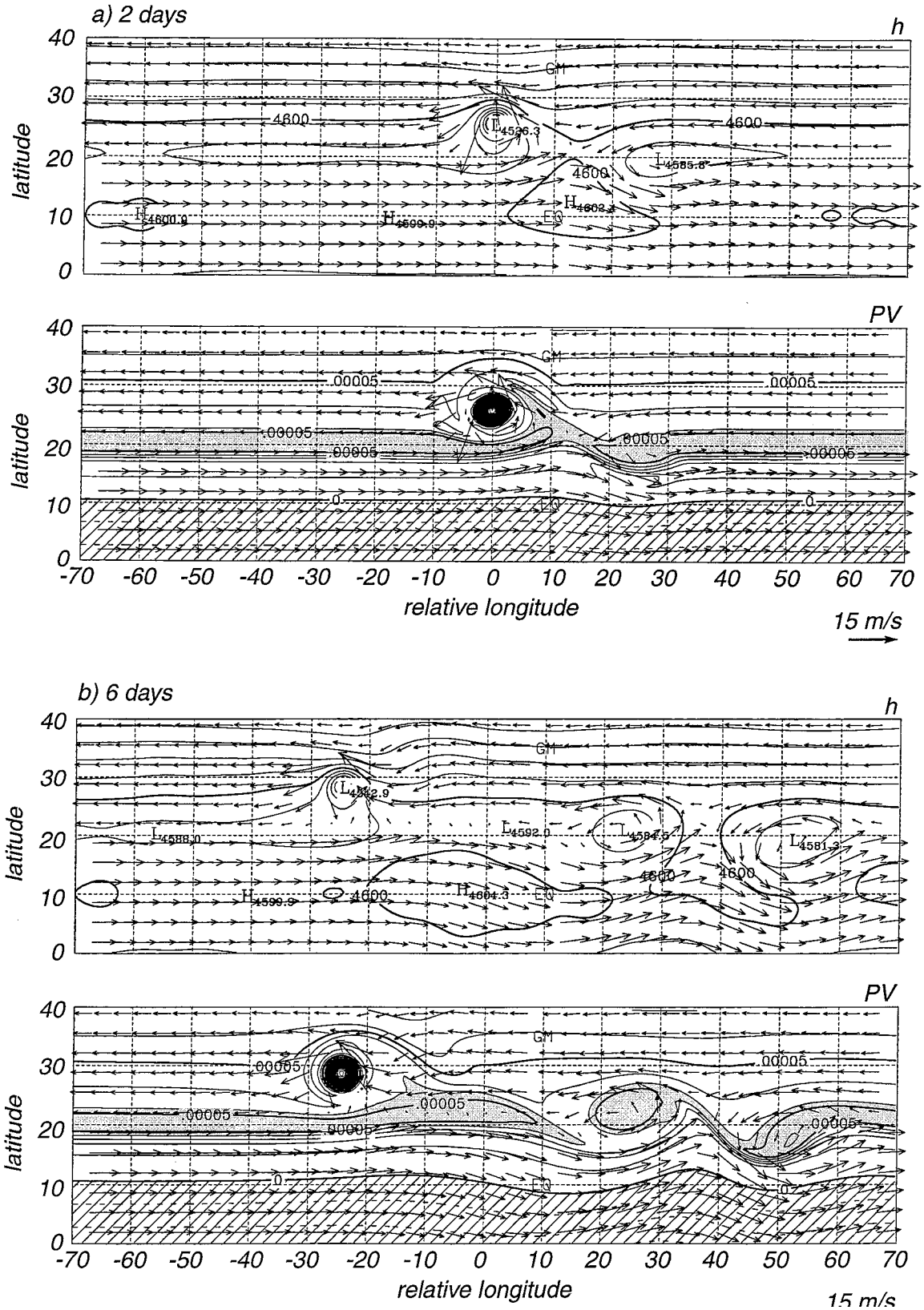

FIG. 8. Interaction of a cyclone centered at 15°N with $\zeta_v = 2.0 \times 10^{-4}$ s^{-1} and 2° in radius with a 4.5° wide zonally symmetric PV strip centered at 10°N with $\zeta_s = 3 \times 10^{-5}$ s^{-1}. The displayed fields are fluid depth (m), PV (s^{-1}), and winds (m s^{-1}) at (a) 2 days, (b) 5 days, and (c) 10 days.

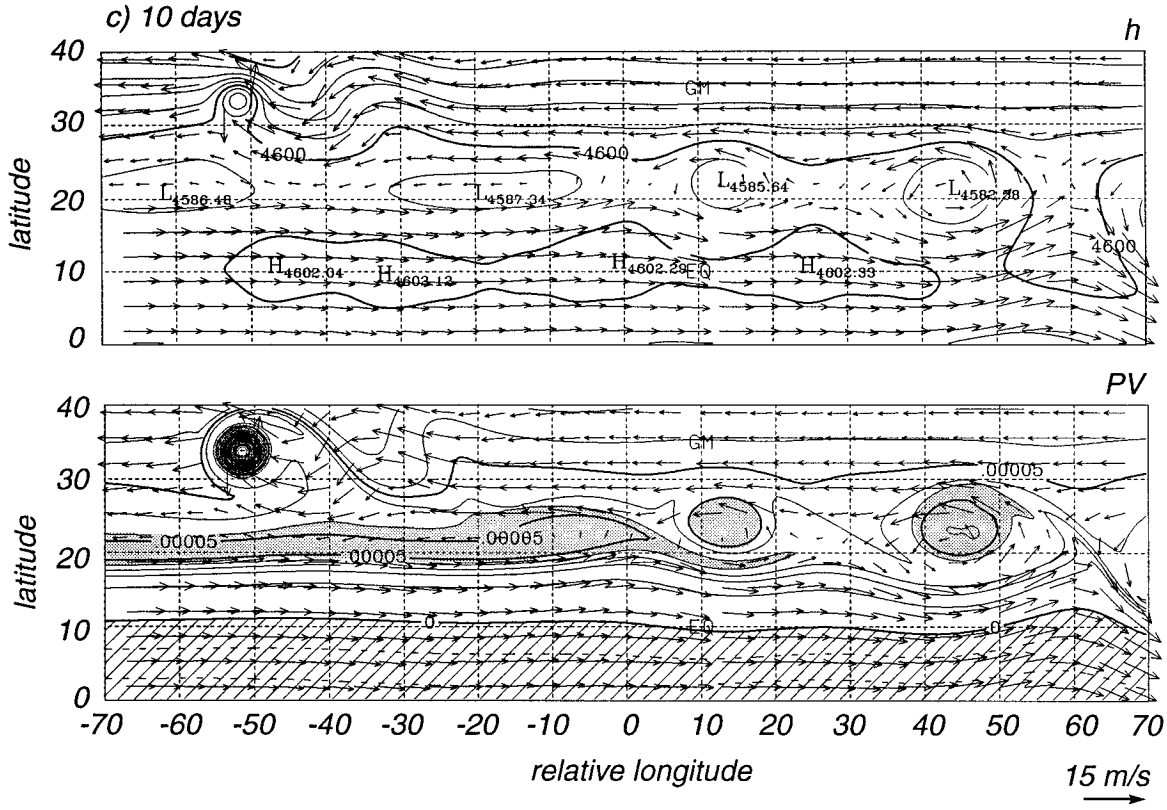

FIG. 8. (*Continued*)

by thin filaments of high PV. The central cyclone is the most intense of the three as is expected from the shape of the PV strip on day 5 (Fig. 11a). After 15 days (Fig. 11d), the PV filaments have dissipated. The asymmetry in flow waviness between the northern and southern sides of the PV strip discussed in section 3 is also present in this experiment. Later on in the simulation (not shown) the two westernmost vortices merged. As seen in Fig. 11d, the trajectories followed by the three cyclones in this experiment had significant meridional components. In contrast, linear normal mode stability theory predicts pure westward propagation of the disturbances produced by barotropic instability.

An interesting feature of the above results is that the zonally elongated mass sink produces the most intense PV anomaly on its poleward side (Fig. 11a). A simple explanation is that the P factor in the $-PQ/h$ term on the right-hand side of Eq. (5) biases the response to the poleward side where the magnitude of P is larger. The cyclones that emerge (e.g., Fig. 11c) are several hundred kilometers poleward of the center of the mass sink. This simple result is entirely consistent with the observational study of Gray (1968), who noted that the typical location of initial disturbance genesis is a few hundred kilometers poleward of the doldrum equatorial trough. In a sense, one might expect cyclones to emerge from the poleward side of an extended zonal strip of ITCZ convection. The bias of the response to the poleward side of the mass sink also indicates the degree of idealization involved in the initial condition used in section 3 (i.e., a strip of constant relative vorticity).

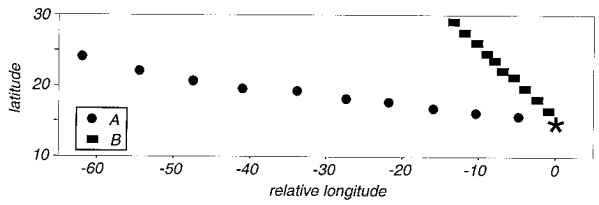

FIG. 9. Trajectories followed by a cyclone centered at 15°N under the influence of a zonally symmetric PV strip centered at 10°N (A). The trajectory of a cyclone centered at 15°N in a quiescent environment (B) is included for comparison. Symbols denote cyclone positions at 24-h intervals.

The importance of using forced experiments in the study of flow stability has been emphasized by Andrews (1984). He showed that the stability of forced, zonally asymmetric flows depends not only on the configuration of the flow but also on the nature of the forcing. This is corroborated by the differences found between the most unstable modes selected in the forced (Fig. 11) and initial value experiments (Fig. 3). Despite the similarity in the shear layer widths produced in these experiments, the wavelength of the most unstable mode

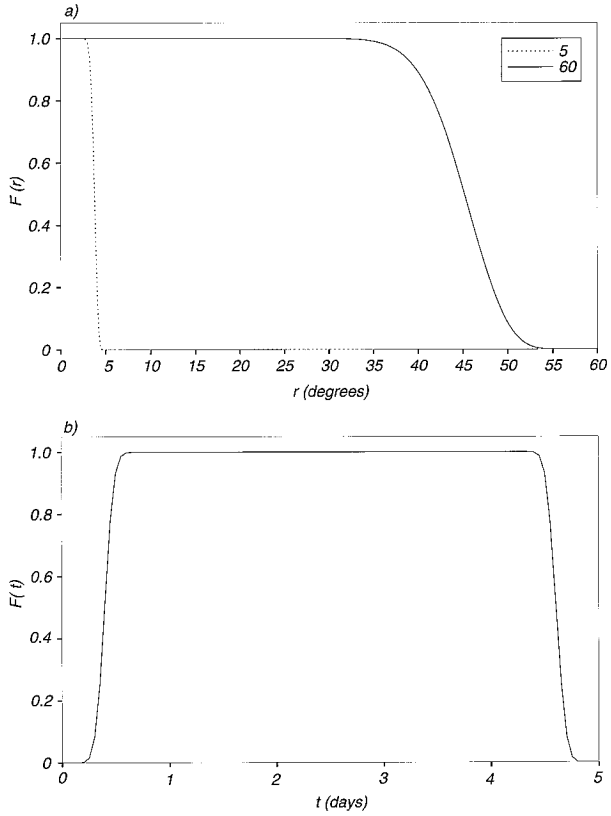

FIG. 10. Nondimensional radial, $\mathcal{F}(r, 30)$, and temporal, $\mathcal{F}(t, 320)$, variation of the mass sink as given by Eq. (10): (a) $\mathcal{F}(r, 30)$ for $c = 5$ and 60 (radius is in degrees from the center of the ellipse); (b) $\mathcal{F}(t, 320)$ for $\tau = 5$ days.

selected in the initial value experiment is almost one and a half times larger than the most unstable mode selected in the forced experiment. The difference persisted when an initial value (Fig. 3) and a forced (not shown) zonally symmetric experiments are compared, giving support to the idea that the nature of the forcing has a strong effect on the stability of the flow.

Figure 12 shows meridional cross sections of the zonal winds through the center of the PV strip on days 5 and 15 of the simulation. In the first 5 days of the simulation, the mass sink produces a flow that resembles the tropical monsoon trough circulation, that is, westerlies to its south and easterlies to its north. This is in agreement with observations (Mapes and Houze 1992) that indicate that the monsoon flow is forced by deep convection. On day 5, note that the westerlies to the south of the PV strip are approximately twice as strong as the easterlies to its north. This difference in strength of the zonal winds is a direct consequence of the meridional variation of inertial stability (e.g., Hack et al. 1989). Since inertial stability decreases toward the equator, it is easier for the mass sink to draw mass from its equatorward than from its poleward side. Hence, stronger meridional winds are found on the equatorward side of the mass sink, resulting in stronger zonal winds through the effect of the Coriolis force. On the equatorward side of the PV strip, an equatorward eddy flux of PV exists (Figs. 11a–c). Wave–mean flow interaction theory (e.g., McIntyre and Norton 1990) shows that an easterly acceleration of the mean flow occurs in such regions. Indeed, as the simulation progresses, easterly winds appear near the equator as seen in Fig. 12 at 15 days. Moreover, the shear layer is displaced northward and its strength decreases as the unstable waves grow at its expense.

Additional simulations (not shown) indicated that the farther the mass sink is placed away from the equator, the faster breakdown will occur. This is expected since the zonal wind shear around the mass sink is produced by the Coriolis force, which is stronger at increasing distances from the equator. Hence, the farther the mass sink is from the equator, the faster the shear region will develop, expediting the breakdown process. In agreement with results from linear stability theory, additional simulations showed that the horizontal dimension of the cyclones that result from breakdown is directly proportional to the PV strip width.

It was also found that the longer the PV strip, the slower its breakdown. In a longer PV strip, the ratio of meridional wind to PV strip size is decreased. The perturbation from zonal asymmetry is therefore smaller and breakdown is slower.

A 40-day long simulation in which the same mass sink was applied twice was performed (not shown) to study two consecutive episodes of ITCZ breakdown and reformation. During the first 20 days, the flow evolution was identical to the evolution shown in Fig. 11. After the mass sink was turned back on at day 20, a new elongated PV strip formed. This second PV strip also broke down into individual cyclones but its evolution was complicated by the background flow in which it was embedded.

6. The breakdown of an irregularly shaped ITCZ

During the northern summer, the ITCZ over the Pacific Ocean is zonally elongated and often wider and more active in its eastern and western ends. This east–west asymmetry in the shape of the ITCZ can be observed in daily satellite images and is present in the climatological distribution of highly reflective clouds shown in Fig. 13. The shape of the ITCZ across the Pacific Ocean is closely tied to the sea surface temperature pattern and the presence of the Asian and American (Horel et al. 1989) continents. In this section, the effect of such asymmetries upon ITCZ breakdown are investigated using idealized zonally elongated mass sinks that are wider at both their eastern and western ends.

A mass sink that is wider on its eastern and western ends is obtained by changing the distortion parameter in Eqs. (12) and (13) to

$$\sigma = 2(p - 1)(\lambda \cos \phi/b)^2/3 + 1.$$

The constant p, which measures the distortion of the mass sink from elliptical symmetry, is half the ratio between the width of the PV strip at $\sqrt{3}c/2$ (or $-\sqrt{3}c/2$) relative longitude and the width at 0° relative longitude. In the first simulation $b = \pi/2$ (corresponding to a 68° half-width for the major axis of the mass sink), $c = \pi/180$ (corresponding to an $\sim 1°$ half-width for the minor axis of the mass sink) and all other constants were kept unchanged.

Figure 14 shows the evolution of the fluid depth, wind, and PV fields produced by an irregularly shaped mass sink with $p = 40$. The shape of the mass sink is outlined by the dots in Fig. 14a. At 5 days (Fig. 14a), a cyclonic PV strip that is wider on its eastern and western sides than at its center has been produced. The flow associated with this PV strip satisfies the necessary condition for the occurrence of barotropic instability. Although the PV strip is nearly symmetric about 0° relative longitude, its eastern and western sides evolve differently. Dispersion of short Rossby waves that originated in the western bulge of the PV strip make the western and central parts of the PV strip (between −65° and 30° relative longitude) undulate and break down into several cyclonic PV pools (see Fig. 14b). As discussed in section 3, the scale of the undulations is directly proportional to the width of the PV strip and decreases from a wavelength of about 2600 km in the western to a wavelength of about 1460 km in the central part of the PV strip. The fact that the weakest and smallest cyclones are found in the central part of the PV strip is in good agreement with observations that show weak easterly wave activity in the central Pacific Ocean (e.g., Nitta et al. 1985). On the eastern side of the PV strip (between 30° and 60° relative longitude), however, axisymmetrization occurs, resulting in only one cyclone whose PV anomaly is horizontally larger and stronger than that of either of the westernmost cyclones (Fig. 14b). The difference in behavior between the eastern and western sides of the PV strips stems from differences in short Rossby wave energy dispersion from these regions.

The formation of Tropical Storm Emilia in the east Pacific Ocean in July 1978 is shown in Fig. 15. On July 3 (Fig. 15a), the ITCZ in the east Pacific is an elongated line of convection that is more active on its eastern side. Tropical Storm Emilia formed on July 6 near the Mexican coast (Fig. 15b; Gunther 1979) and reached its peak intensity on July 9 (Fig. 15c). In a qualitative sense, the evolution of the eastern end of the PV strip in Fig. 14 resembles the evolution of the ITCZ during the formation of Tropical Storm Emilia. The flow evolution seen in Fig. 14 along with the climatological shape of the ITCZ in the eastern Pacific suggest that axisymmetrization of the flow produced by ITCZ convection may play a role in producing the observed high concentration of tropical cyclogenesis near the west coast of Central America (e.g., Gray 1968; Zehnder 1991). An alternative explanation for the time and space clustering of tropical cyclogenesis in the eastern Pacific has been put forth by Zehnder (1991) and Zhong et al. (1993) and involves an interaction of a quasi-persistent favorable large-scale flow with the Sierra Madre.

A series of simulations has been performed to study the behavior of PV strips with different values of p and b. The results are summarized in Fig. 16. It is seen that the longer the PV strip (or the larger b), the larger the distortion, p, needed for axisymmetrization to prevail over breakdown on the eastern side of the PV strip. On the western side of the PV strip, however, breakdown is a robust behavior and axisymmetrization did not occur for the range of parameters (b and p) studied. The effect of varying the value of p for $b = \pi/2$ upon the shape of the mass sink is shown in the left part of Fig. 16.

The results obtained in the forced simulations point to the importance of zonal asymmetries in the formation of tropical disturbances through barotropic instability. The main effect of zonal asymmetries appears to be in the size and movement of the resulting cyclones, as well as in the type of evolution that leads to their formation. The effect of zonal asymmetries upon the stability of barotropic flows has previously been studied for easterly (e.g., Tupaz et al. 1978; Williams et al. 1984; Peng and Williams 1986) and westerly (e.g., Mak and Cai 1989) jets. The main result of these studies is that the fastest growth of the unstable modes occurs in the downstream region of the jet. It would be of interest to know what results such stability studies would produce for a shear layer meridional profile of zonal wind such as the ones produced by ITCZ convection.

7. Concluding remarks

Easterly waves occur in many tropical regions and result from a convectively modified form of combined barotropic and baroclinic instability of the mean zonal flow. ITCZ convection plays an important role in the origin of the unstable mean flow in which easterly waves form. In the lower troposphere, ITCZ convection produces a cyclonic PV anomaly that satisfies the necessary, but not sufficient, condition for combined barotropic and baroclinic instability. The unstable ITCZ may then break down into a series of tropical disturbances within which tropical cyclones may form, provided that favorable environmental conditions exist. In this study, a shallow-water model on the sphere was used to study barotropic aspects of ITCZ breakdown.

Initial value simulations in which the ITCZ was idealized as a zonally symmetric PV strip were performed. The breakdown of the PV strip was in good agreement with linear normal mode stability analysis. Moreover, an asymmetry between the amplitude of the waves on the northern and southern sides of the PV strip occurred. This asymmetry was found to be an effect of the planetary vorticity gradient, which causes the isolines of PV

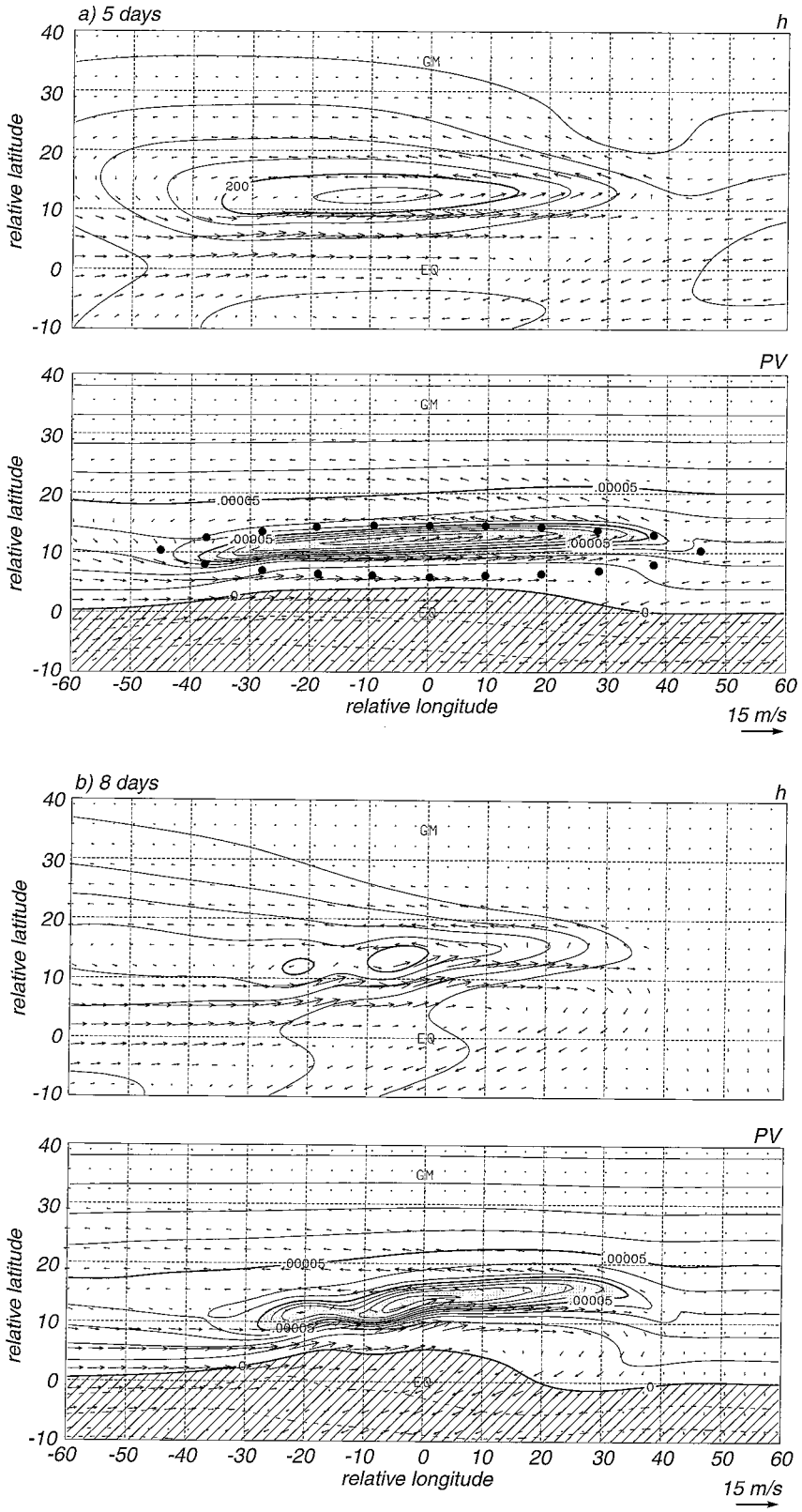

FIG. 11. Evolution of the flow field in response to a zonally elongated mass sink centered at 10°N latitude and 0° longitude. The shape and position of the mass sink are indicated by the dots in the PV field at 5 days. The displayed fields are fluid depth (m), PV (s^{-1}), and winds (m s^{-1}) at (a) 5 days, (b) 8 days, (c) 11 days, and (d) 15 days. Superimposed on the PV fields at 15 days are the trajectories that the vortices followed between days 15 and 23. Dots denote cyclone positions at 2-day intervals.

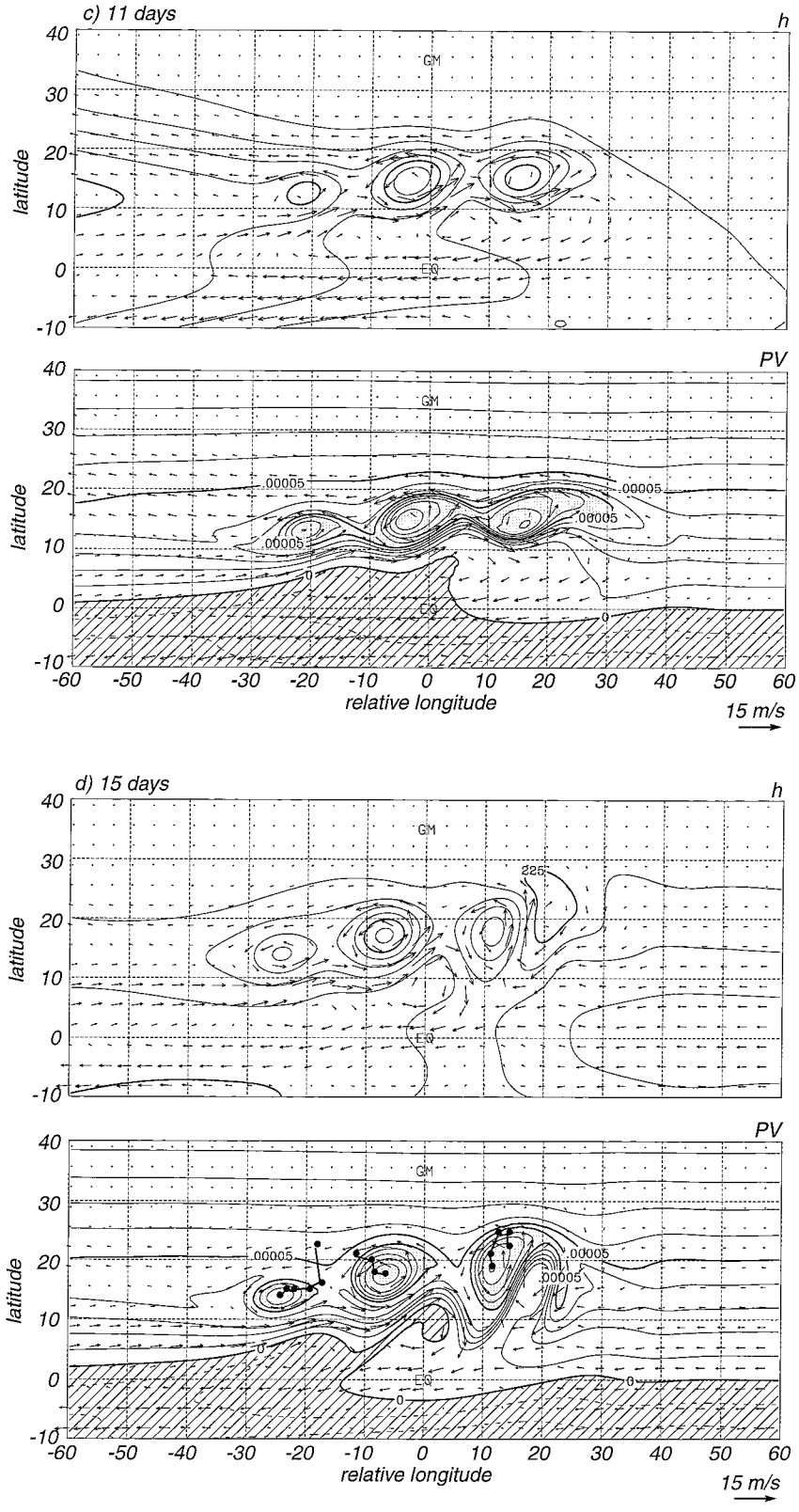

FIG. 11. (*Continued*)

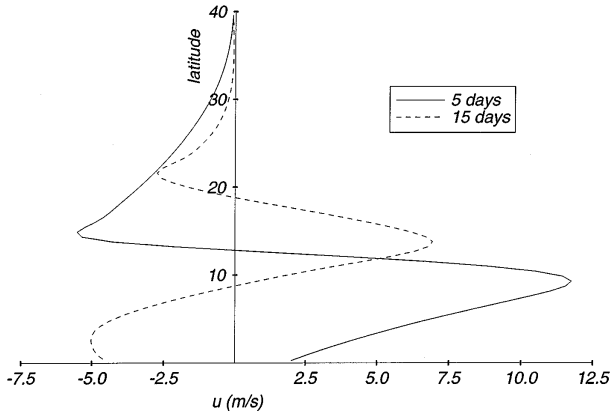

FIG. 12. Meridional profiles of zonal winds across the center of the PV strip after 5 and 15 days.

to be more closely packed on the southern than on the northern side of the PV strip. The existence of such an asymmetry in nature has yet to be confirmed. When a cyclone was introduced just to the north of the PV strip, short Rossby wave dispersion to the east of the cyclone perturbed the zonally symmetric PV strip, promoting its breakdown.

More realistic experiments simulated the effect of ITCZ convection upon the circulation of the lower troposphere by zonally elongated mass sinks of various shapes and dimensions. A common feature to all of the forced simulations was the formation, in a few model days, of cyclonic PV anomalies that were biased to the poleward side of the mass sink and obeyed the necessary condition for the occurrence of barotropic instability. A shear layer flow pattern was associated with these PV strips. In agreement with linear stability analysis, an elliptical mass sink produced a PV strip that broke down into a series of cyclones whose dimensions and number were directly proportional to the dimensions of the mass sink. In addition, the cyclones formed sequentially from west to east. When the mass sink was made wider on its western and eastern ends than at its center, it produced a similarly shaped PV strip. Despite the symmetry of the PV strip about its central longitude, its eastern and western sides behaved differently. The western side of the PV strip tended to break down into a number of cyclones for a wide range of departures from elliptical symmetry. This occurs because dispersion of short Rossby wave energy to the east of the western bulge of the PV strip makes the PV strip undulate, triggering breakdown. On the eastern side of the PV strip, axisymmetrization into one large cyclone dominated over breakdown beyond a certain degree of departure from elliptical symmetry.

The presence of zonal asymmetries in the modeled ITCZ affected the size, movement, and mode of formation of the resulting cyclones. This illustrates the

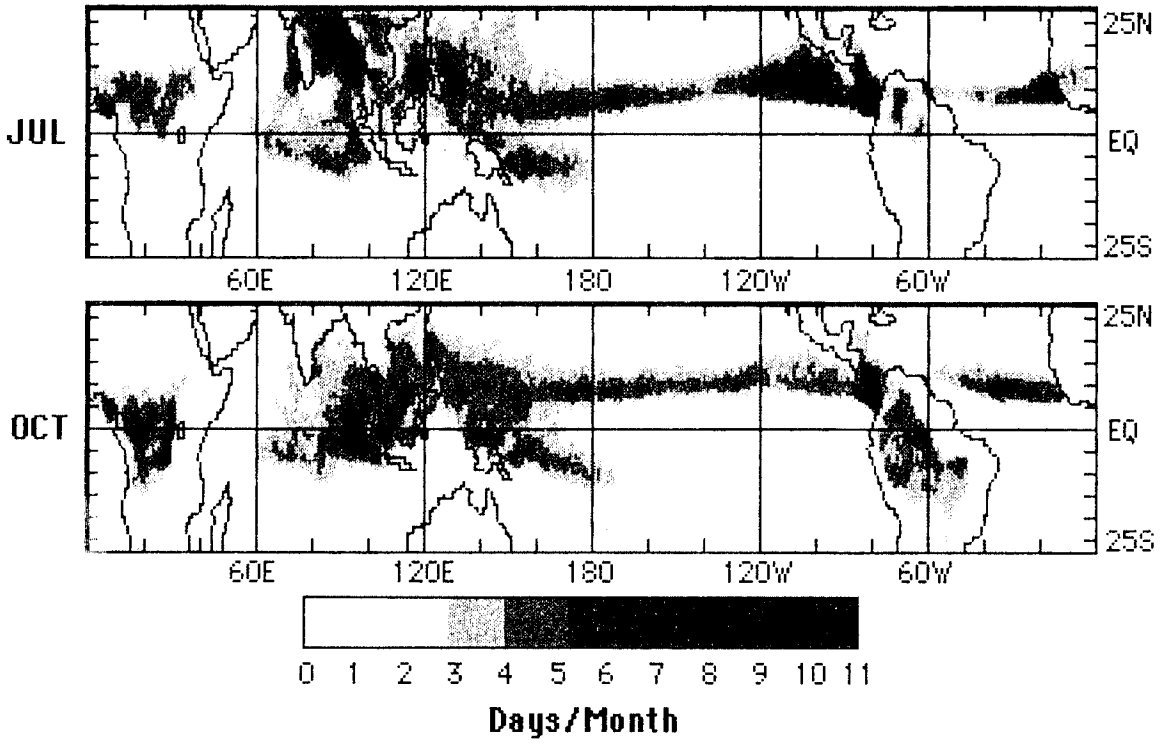

FIG. 13. Mean monthly ITCZ structure for July and October based on 17 years of monthly highly reflective cloud data. Values represent the number of days per month that a given grid point was covered by a large-scale convective system. From Waliser and Gautier (1993).

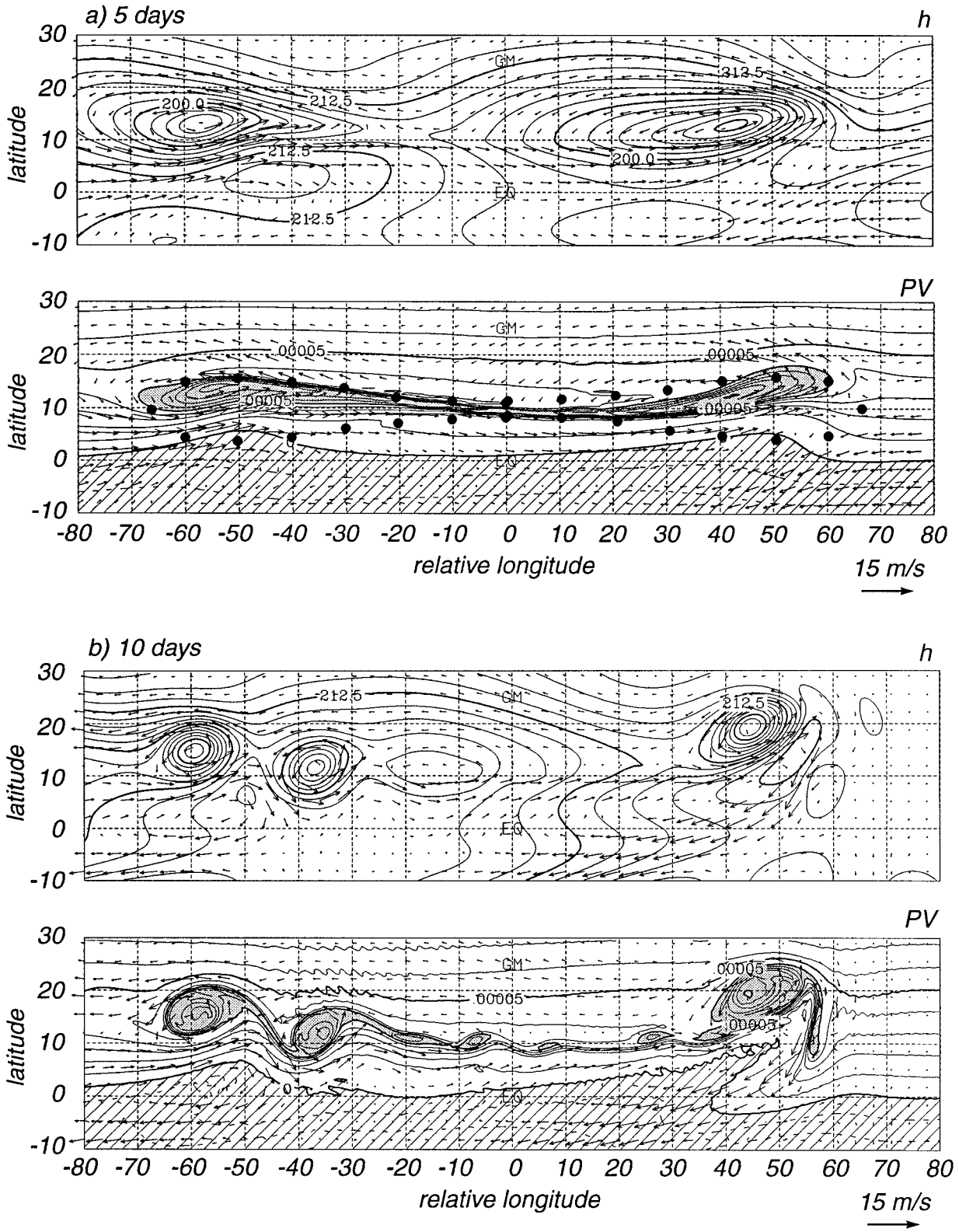

FIG. 14. Evolution of the flow field in response to a zonally oriented, irregularly shaped mass sink with $p = 40$ and $b = \pi/2$. The shape and position of the mass sink are indicated by the dots in the PV field at 5 days. The displayed fields are fluid depth (m), wind (m s^{-1}), and PV (s^{-1}) at (a) 5 days and (b) 10 days.

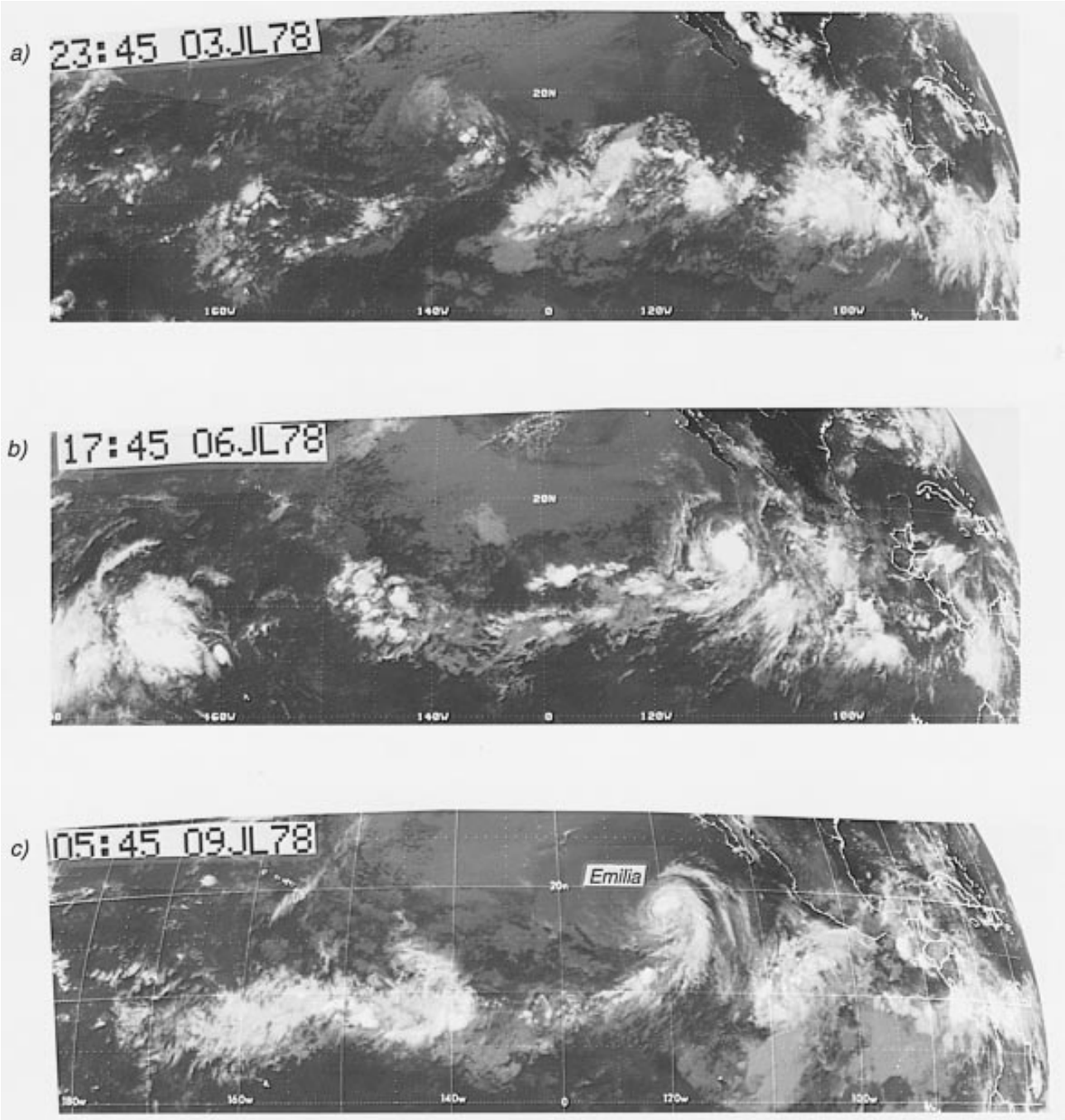

FIG. 15. GOES IR satellite images for 3, 6, and 9 July 1978, showing the formation of Tropical Storm Emilia (time is UTC).

importance of large-scale zonal asymmetries that are inherent to the ITCZ in determining the flow evolution and points to the need for further studies of these effects. The importance of using forced simulations in the study of flow instability was also evident in the simulations shown in this study. Not only do forced simulations address the origin of the unstable flow, but the nature of the forcing can change the characteristics of the most unstable modes.

The lack of observations in tropical oceanic regions makes the study of PV anomalies in nature difficult. Evidence for the existence of zonally elongated PV and relative vorticity strips in the lower troposphere in the Pacific Ocean, Caribbean Sea, and Northern Africa exists in time means of European Centre for Medium-Range Weather Forecasts analyses (e.g., Nitta and Takayabu 1985; Tai and Ogura 1987; Molinari et al. 1997).

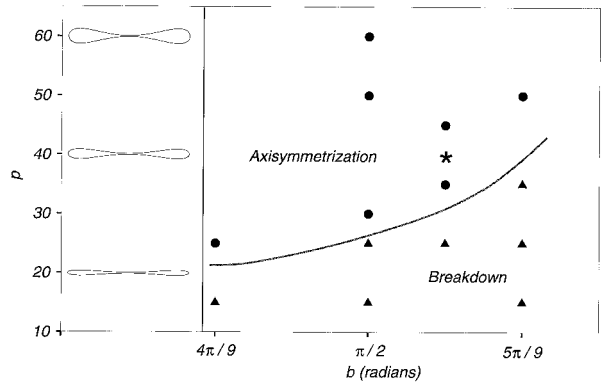

FIG. 16. Behavior of the eastern side of the PV strip produced by the irregularly shaped mass sink as a function of PV strip half-length b and distortion from elliptical symmetry p. The shape of the mass sink for $b = \pi/2$ and different values of p is shown in the left part of the diagram. Solid dots and the star indicate combinations of b and p that lead to axisymmetrization of the eastern half of the PV anomaly. Triangles indicate combinations of b and p that lead to breakdown of the eastern half of the PV anomaly into two or more cyclones. The experiment shown in Fig. 14 is denoted by the star. The western side of the PV broke down into two or more cyclones for all combinations of b and p simulated.

Indirect evidence for the occurrence in nature of the modeled circulations exists: 1) the observed tendency for tropical disturbance formation just to the north of the monsoonal equatorial trough is consistent with the formation of the most intense PV anomaly and the formation of cyclones on the poleward side of the modeled mass sink; 2) axisymmetrization of the flow produced by an ITCZ that is wider on its eastern end may play a role in explaining the large number of tropical storms that occur in the eastern Pacific near Central America; 3) Rossby wave energy dispersion and/or ITCZ breakdown may cause the observed tendency for new tropical storms to form to the east of existing ones (this tendency may also simply be an artifact of the movement of tropical cyclones away from their preferred origin regions); and 4) the weak easterly wave activity in the central Pacific may reflect the relative weakness of the ITCZ and PV anomalies in that region. Further work is needed to investigate the validity of these hypotheses.

Since ITCZ breakdown tends to produce several tropical disturbances in an interval of a few days and within a few degrees from each other, it is plausible that successive episodes of ITCZ breakdown and reformation play a role in the observed global time clustering of tropical cyclones. Gray (1979) observed a global tendency for tropical cyclones to cluster in time, with active tropical cyclone periods lasting about 1–2 weeks, followed by 2–4-week long inactive periods. He proposed that large-scale, slowly varying anomalies [such as the Madden–Julian oscillation in the Indian and Western Pacific Oceans; Liebmann et al. (1994)] alter environmental genesis parameters such as to hinder or enhance cyclogenesis, resulting in the observed time clustering.

In the eastern Pacific in particular, ITCZ breakdown may be initiated and/or accelerated by Atlantic easterly waves that cross Central America. However, separating the role of local ITCZ breakdown from that of Atlantic easterly waves in generating tropical cyclones in the east Pacific could be an observationally difficult task since the time and space scales of the two processes are comparable.

The shallow-water model captures some important barotropic aspects of the dynamics of the formation of tropical disturbances through ITCZ breakdown. The main limitations of this study are imposed by the absence of moist processes and vertical stratification, and the use of highly idealized initial states and forcings. The mass sinks used in this paper are highly idealized proxies for ITCZ convection. For instance, they do not explicitly resolve the smaller scales of convection of which the ITCZ is composed. However, it is expected that these smaller scales of convection will produce finer-scale features in the PV fields whose inversion would result in smooth circulations much like the ones discussed in this paper. It should be emphasized that our results do not imply that barotropic instability is the sole process involved in ITCZ breakdown. Indeed, ITCZ breakdown involves an interplay of barotropic, baroclinic, and moist physical processes. Finally, the nearly symmetric pooled regions of high PV formed in the simulations shown here are far from the intensity of tropical cyclones. They would require a substantial diabatic boost in their PV to reach such intensity.

Acknowledgments. We would like to express our sincere thanks to James Hack of NCAR/CGD for his advice on the use of his shallow-water model. We have benefited greatly from the comments of Paul Ciesielski, William Gray, Richard Johnson, Michael Montgomery, David Randall, Thomas Rickenbach, Lloyd Shapiro, Richard Taft, Gerald Taylor, Chris Thorncroft, and Raymond Zehr. The present research was supported by CNPq, the Brazilian Council for the Development of Science and Technology, and by NOAA through TOGA/COARE Grant NA37RJ0202.

APPENDIX A

Numerical Aspects of the Shallow-Water Model

The shallow-water equations (1)–(3) form a closed system in u, v, and h. An equivalent closed system in δ, ζ, and h is obtained by replacing the momentum equations with the divergence and vorticity equations. This divergence/vorticity form, which is the form actually used in the numerical model, can be written as

$$\frac{\partial \delta}{\partial t} - \frac{\partial(\zeta V)}{a(1 - \mu^2)\partial\lambda}$$

$$+\frac{\partial(\zeta U)}{a\partial\mu}+\nabla^2\left[gh+\frac{U^2+V^2}{2(1-\mu^2)}\right]=-K\left(\nabla^4\delta-\frac{4}{a^4}\delta\right), \tag{A1}$$

$$\frac{\partial\zeta}{\partial t}+\frac{\partial(\zeta U)}{a(1-\mu^2)\partial\lambda}+\frac{\partial(\zeta V)}{a\partial\mu}=-K\left(\nabla^4\zeta-\frac{4}{a^4}\zeta\right), \tag{A2}$$

$$\frac{\partial h}{\partial t}+\frac{\partial(hU)}{a(1-\mu^2)\partial\lambda}+\frac{\partial(hV)}{a\partial\mu}=Q-K\nabla^4 h, \tag{A3}$$

where K is a hyperdiffusion coefficient and

$$\delta=\frac{\partial U}{a(1-\mu^2)\partial\lambda}+\frac{\partial V}{a\partial\mu}, \tag{A4}$$

$$\zeta=2\Omega\mu+\frac{\partial V}{a(1-\mu^2)\partial\lambda}-\frac{\partial U}{a\partial\mu}, \tag{A5}$$

with $U=u\cos\phi$, $V=v\cos\phi$, and $\mu=\sin\phi$. Hyperdiffusion has been added to control spectral blocking (i.e., accumulations on the smallest resolved scales) while increasing the inertial range of the flow; the undifferentiated terms on the right-hand sides of (A1) and (A2) prevent damping of solid-body rotation. Although hyperdiffusion causes spurious oscillations in the vorticity field outside PV patches (Jiménez 1994), this effect is not expected to be important in the T213 simulations presented here.

The horizontal velocity may be written as the sum of divergent and rotational parts; that is,

$$U=\frac{\partial\chi}{a\partial\lambda}-(1-\mu^2)\frac{\partial\psi}{a\partial\mu}, \tag{A6}$$

$$V=(1-\mu^2)\frac{\partial\chi}{a\partial\mu}+\frac{\partial\psi}{a\partial\lambda}, \tag{A7}$$

where χ and ψ are a scalar velocity potential and streamfunction, respectively. The prognostic variables δ and ζ can be expressed as functions of χ and ψ by substituting (A6) and (A7) into (A4) and (A5) to obtain

$$\delta=\nabla^2\chi, \tag{A8}$$

$$\zeta=2\Omega\mu+\nabla^2\psi. \tag{A9}$$

The use of (A8) and (A9) eases matters because the Laplacian operator has a simple form in the spectral space whose basis functions are spherical harmonics.

Substitution of (A6)–(A9) into (A1)–(A3) yields a nonlinear system of prognostic equations for ψ, χ, and h that is solved using the spectral transform method in space and semi-implicit time differencing. In the spectral method the horizontal structure of the dependent variables is represented by series expansions in terms of spherical harmonics $P_n^m(\mu)e^{im\lambda}$, where P_n^m is the associated Legendre function, m the zonal wavenumber, and n the total wavenumber, with $0\le|m|\le n$. In the simulations shown in this study, triangular truncation $0\le n\le N$, with $N=213$, was used. In each time step nonlinear terms and diabatic processes are calculated in the transform grid, and linear terms, derivatives, and time tendencies are evaluated in spectral space. For more information on the numerical aspects of the model, see Hack and Jakob (1992) and Jakob-Chien et al. (1995).

Time integration of the shallow-water model requires knowledge of the initial fields of either ζ, δ, and h or U, V, and h on the transform grid. The model initialization is straightforward in cases where the initial wind fields are at rest and the fluid depth is constant. If the initial state is not at rest, the model should be initialized with balanced mass and wind fields in order to keep transient gravity waves to a minimum. In the model simulations shown here, given the initial vorticity, the wind and geopotential fields are obtained therefrom as follows. First, the streamfunction ψ is obtained from the vorticity through (A9). The corresponding nondivergent wind field is then computed from

$$U=-(1-\mu^2)\frac{\partial\psi}{a\partial\mu}\quad\text{and}\quad V=\frac{\partial\psi}{a\partial\lambda}. \tag{A10}$$

It is then assumed that the mass and wind fields obey a nonlinear balance relation (Charney 1960), which is obtained by neglecting the hyperdiffusion and the local time derivative of divergence in (A1), resulting in

$$g\nabla^2 h=\frac{\partial(V\zeta)}{a(1-\mu^2)\partial\lambda}-\frac{\partial(U\zeta)}{a\partial\mu}-\nabla^2\left[\frac{U^2+V^2}{2(1-\mu^2)}\right]. \tag{A11}$$

In summary, given an initial vorticity field, (A9) is used to compute the initial ψ, (A10) to compute the initial U and V, and (A11) to compute the initial h. The nonlinear terms in these equations are calculated in physical space and the remaining terms are most easily computed in spectral space.

The value chosen for the hyperdiffusion coefficient is $K=8.0\times10^{12}$ m^4 s^{-1}. This choice is sufficient to prevent spectral blocking and to give a reasonably straight tail to the kinetic energy spectra (Jakob-Chien et al. 1995). It results in a damping time of 27.5 h for the $n=213$ spherical harmonic coefficients and a damping time of 444 h for the $n=106$ coefficients.

APPENDIX B

Three Region Model

Consider the nondivergent barotropic vorticity equation on a β plane, linearized about a basic-state zonal flow $\bar{u}$ that varies with latitude. This equation has the form

$$\left(\frac{\partial}{\partial t}+\bar{u}\frac{\partial}{\partial x}\right)\nabla^2\psi+\frac{\partial\psi}{\partial x}\frac{d\bar{\zeta}}{dy}=0, \tag{B1}$$

where $\bar{\zeta}(y) = f_0 + \beta y - \bar{u}_y$, and ψ is the streamfunction for the perturbation horizontal velocity components $u' = -\partial\psi/\partial y$ and $v' = \partial\psi/\partial x$, in which case the perturbation vorticity is $\nabla^2\psi$. We shall search for solutions of (B1) having the form $\psi(x, y, t) = \Psi(y)e^{ik(x-ct)}$, where k is the zonal wavenumber and c can be complex. Equation (B1) becomes

$$\frac{d^2\Psi}{dy^2} + \left(\frac{\beta - \bar{u}_{yy}}{\bar{u} - c} - k^2\right)\Psi = 0. \tag{B2}$$

Following the classic approach described by Rayleigh (1945, 392–394) and Gill (1982, section 13.6), let us consider a three-region model in which the basic-state zonal flow has the form

$$\bar{u}(y) = \begin{cases} -U + \dfrac{\beta}{2}(y - y_0)^2, & y_0 \le y < \infty \\ -U\dfrac{y}{y_0} + \dfrac{\beta}{2}(y^2 - y_0^2), & -y_0 \le y \le y_0 \\ U + \dfrac{\beta}{2}(y + y_0)^2, & -\infty < y \le -y_0, \end{cases} \tag{B3}$$

where U and y_0 are specified constants. This is essentially a shear layer flow with $\bar{u}(y_0) = -U$ and $\bar{u}(-y_0) = U$. The corresponding piecewise constant basic-state absolute vorticity $\bar{\zeta}(y)$ is therefore given by

$$\bar{\zeta}(y) = f_0 + \beta y - \frac{d\bar{u}}{dy} = \begin{cases} f_0 + \beta y_0, & y_0 \le y < \infty \\ f_0 + \dfrac{U}{y_0}, & -y_0 \le y \le y_0 \\ f_0 - \beta y_0, & -\infty < y \le -y_0. \end{cases} \tag{B4}$$

The central region ($-y_0 \le y \le y_0$) represents an ITCZ that lies north of the equator. Large positive absolute vorticity occurs in the ITCZ region. At $y = -y_0$ there is a concentrated positive gradient of absolute vorticity, while at $y = y_0$ there is a concentrated negative gradient of absolute vorticity.

Except along the lines $y = \pm y_0$, $\bar{\zeta}_y = \beta - \bar{u}_{yy} = 0$, so from (B2), we conclude that $d^2\Psi/\partial y^2 - k^2\Psi = 0$. Thus, nonzero perturbation vorticity occurs only along $y = \pm y_0$, with the perturbation flow being irrotational elsewhere. As solutions of (B2), which are bounded as $|y| \to \infty$, we have

$$\psi(x, y, t) = (\Psi_s e^{-k|y+y_0|} + \Psi_n e^{-k|y-y_0|})e^{ik(x-ct)}, \tag{B5}$$

where Ψ_s and Ψ_n are constants. Note from (B5) that ψ and hence $v' = \partial\psi/\partial x$ are continuous at $y = \pm y_0$. The solution associated with the constant Ψ_s has vorticity anomalies concentrated at $y = -y_0$, so that the corresponding solution for ψ decays away in both directions from $y = -y_0$. Similarly, the solution associated with the constant Ψ_n has vorticity anomalies concentrated at $y = y_0$ and the corresponding solution for ψ decays away from $y = y_0$. Integrating (B2) over a narrow region centered on either $y = -y_0$ or $y = y_0$ gives

$$(\bar{u} - c)\Delta\left(\frac{d\Psi}{dy}\right) + \Psi\Delta\bar{\zeta} = 0 \quad \text{at} \quad y = \pm y_0, \tag{B6}$$

where Δ stands for the jump across the narrow region. Substituting (B5) into (B6) yields

$$-c_n e^{-2ky_0}\Psi_s + (c + U - c_n)\Psi_n = 0, \tag{B7}$$

$$(-c + U + c_s)\Psi_s + c_s e^{-2ky_0}\Psi_n = 0, \tag{B8}$$

where

$$c_s = -\frac{U(b + 1)}{2ky_0}, \qquad c_n = -\frac{U(b - 1)}{2ky_0}, \qquad b = \frac{\beta y_0^2}{U}.$$

If the basic-state vorticity jump at the southern interface was removed, the first term in (B7) would disappear and the Rossby wave on the northern interface would propagate with phase speed $c = -U + c_n$. Similarly, if the basic-state vorticity jump at the northern interface was removed, the second term in (B8) would disappear and the Rossby wave on the southern interface would propagate with phase speed $c = U + c_s$. For a typical active monsoon situation, $U > 0$ and $0 < b < 1$, so that $c_s < 0$ and $c_n > 0$; that is, the noninteracting Rossby wave on the northern interface propagates eastward relative to the easterly zonal flow on the reversed poleward gradient of basic-state vorticity, while the noninteracting Rossby wave on the southern interface propagates westward relative to the westerly zonal flow on the normal poleward gradient of basic-state vorticity. Hence, the system (B7)–(B8) can be regarded as a concise mathematical description of the interaction of two counterpropagating Rossby waves and, ultimately, of barotropic instability (Hoskins et al. 1985, section 6b). The first term in (B7) gives the effect of the southern vorticity anomaly pattern on the behavior of the northern interface, while the second term in (B8) gives the effect of the northern vorticity anomaly pattern on the behavior of the southern interface. Note that the effect of these interactions decays with increasing wavenumber and increasing shear layer width according to e^{-2ky_o}.

Regarding (B7) and (B8) as a linear homogeneous system in the unknowns Ψ_s and Ψ_n, the requirement that the determinant of the coefficients vanish yields the eigenvalue relation

$$\frac{ky_0c}{U} = -\frac{1}{2}b \pm \left[\left(\frac{1}{2} - ky_0\right)^2 + \frac{1}{4}(b^2 - 1)e^{-4ky_0}\right]^{1/2}. \tag{B9}$$

From (B9) we note that $|b| < 1$ is a necessary condition for instability. For unstable flows the dimensionless phase speed and growth rate are

$$\frac{c_r}{U} = -\frac{b}{2ky_0},$$

$$\frac{kc_i}{\beta y_0} = \frac{1}{b}\left[\frac{1}{4}(1 - b^2)e^{-4ky_0} - \left(\frac{1}{2} - ky_0\right)^2\right]^{1/2}. \quad \text{(B10)}$$

Note that $c_r = (c_n + c_s)/2$; that is, the phase speed of the barotropically unstable disturbance is simply the average speed of the noninteracting Rossby waves on the two interfaces.

If we calculate the complex eigenvalue c from (B9), use this result in (B7) or (B8) to determine the ratio between Ψ_s and Ψ_n, and then use this ratio in (B5), we will have determined the corresponding eigenfunction ψ to within a multiplicative constant. This procedure results in the eigenfunction displayed in Fig. 4. The total streamfunction is displayed in Fig. 4a and the parts associated with Ψ_n and Ψ_s in Figs. 4b and 4c. The β effect causes a larger streamfunction anomaly on the equatorward side of the PV strip.

REFERENCES

Agee, E. M., 1972: Note on ITCZ wave disturbances and formation of Tropical Storm Anna. *Mon. Wea. Rev.,* **100,** 733–737.

Andrews, D. G., 1984: On the stability of forced non-zonal flows. *Quart. J. Roy. Meteor. Soc.,* **110,** 657–662.

Avila, L. A., and G. B. Clark, 1989: Atlantic tropical systems of 1988. *Mon. Wea. Rev.,* **117,** 2260–2265.

Burpee, R. W., 1972: The origin and structure of easterly waves in the lower troposphere of North Africa. *J. Atmos. Sci.,* **29,** 77–90.

——, 1975: Some features of synoptic-scale waves based on a compositing analysis of GATE data. *Mon. Wea. Rev.,* **103,** 921–925.

Carlson, T. N., 1969: Synoptic histories of three African disturbances that developed into Atlantic hurricanes. *Mon. Wea. Rev.,* **97,** 256–276.

Chan, J. C. L., and R. T. Williams, 1987: Analytical and numerical studies of the beta-effect in tropical cyclone motion. Part I: Zero mean flow. *J. Atmos. Sci.,* **44,** 1257–1265.

Chang, C., 1970: Westward propagating cloud patterns in the tropical Pacific as seen from time-composite satellite photographs. *J. Atmos. Sci.,* **27,** 133–138.

Charney, J. G., 1960: Integration of the primitive and balance equations. *Proc. Int. Symp. on Numerical Weather Prediction,* Tokyo, Japan, Meteor. Soc. Japan, 131–152.

——, and M. E. Stern, 1962: On the stability of internal baroclinic jets in a rotating atmosphere. *J. Atmos. Sci.,* **19,** 159–172.

Chen, W.-L., and Y. Ogura, 1982: Modulation of convective activity by large-scale flow patterns observed in GATE. *J. Atmos. Sci.,* **39,** 1260–1279.

Drazin, P. G., and W. H. Reid, 1981: *Hydrodynamic Instability.* Cambridge University Press, 527 pp.

Dritschel, D. G., 1989: On the stabilization of a two-dimensional cyclone strip by adverse shear. *J. Fluid Mech.,* **206,** 193–221.

——, and L. M. Polvani, 1992: The roll-up of vorticity strips on the surface of a sphere. *J. Fluid Mech.,* **234,** 47–69.

——, P. H. Haynes, M. N. Juckes, and T. G. Shepherd, 1991: The stability of a two-dimensional vorticity filament under uniform strain. *J. Fluid Mech.,* **230,** 647–665.

Evans, J. L., G. J. Holland, and R. L. Elsberry, 1991: Interactions between a barotropic cyclone and an idealized subtropical ridge. Part I: Vortex motion. *J. Atmos. Sci.,* **48,** 301–314.

Frank, N. L., 1969: The ''inverted V'' cloud pattern—An easterly wave? *Mon. Wea. Rev.,* **97,** 130–140.

Frank, W. M., 1982: Large-scale characteristics of tropical cyclones. *Mon. Wea. Rev.,* **110,** 572–586.

Fulton, S. R., and W. H. Schubert, 1985: Vertical normal mode transforms: Theory and application. *Mon. Wea. Rev.,* **113,** 647–658.

Gerrish, H. P., and M. Mayfield, 1989: Eastern North Pacific tropical cyclones of 1988. *Mon. Wea. Rev.,* **117,** 2266–2277.

Gill, A. E., 1982: *Atmosphere–Ocean Dynamics.* Academic Press, 662 pp.

Gray, W. M., 1968: Global view of the origin of tropical disturbances and storms. *Mon. Wea. Rev.,* **96,** 669–700.

——, 1979: Hurricanes: Their formation, structure and likely role in the tropical circulation. *Meteorology over the Tropical Oceans,* D. B. Shaw, Ed., Roy. Meteor. Soc., 155–218.

Guinn, T. A., and W. H. Schubert, 1993: Hurricane spiral bands. *J. Atmos. Sci.,* **50,** 3380–3403.

Gunther, E. B., 1979: Eastern North Pacific tropical cyclones of 1978. *Mon. Wea. Rev.,* **107,** 911–927.

Hack, J. J., and R. Jakob, 1992: Description of a global shallow water model based on the transform method. NCAR Tech. Note (NCAR/TN-343+STR), 39 pp. [Available from Climate and Global Dynamics Division, NCAR, P.O. Box 3000, Boulder, CO 80307]

——, W. H. Schubert, D. E. Stevens, and H.-C. Kuo, 1989: Response of the Hadley circulation to convective forcing in the ITCZ. *J. Atmos. Sci.,* **46,** 2957–2973.

Heta, Y., 1991: On the origin of tropical disturbances in the equatorial Pacific. *J. Meteor. Soc. Japan,* **69,** 337–351.

Holland, G. J., 1995: Scale interaction in the western Pacific monsoon. *Meteor. Atmos. Phys.,* **56,** 57–79.

Horel, J. D., A. N. Hahmann, and J. E. Geisler, 1989: An investigation of the annual cycle of convective activity over the tropical Americas. *J. Climate,* **2,** 1388–1403.

Hoskins, B. J., A. J. Simmons, and D. G. Andrews, 1977: Energy dispersion in a barotropic atmosphere. *Quart. J. Roy. Meteor. Soc.,* **103,** 553–567.

——, M. E. McIntyre, and A. W. Robertson, 1985: On the use and significance of isentropic potential vorticity maps. *Quart. J. Roy. Meteor. Soc.,* **111,** 877–946.

Jakob-Chien, R. J., J. J. Hack, and D. L. Williamson, 1995: Spectral transform solutions to the shallow water test set. *J. Comput. Phys.,* **119,** 164–187.

Jiménez, J., 1994: Hyperviscous vortices. *J. Fluid Mech.,* **279,** 169–176.

Joly, A., and A. J. Thorpe, 1990: Frontal instability generated by tropospheric potential vorticity anomalies. *Quart. J. Roy. Meteor. Soc.,* **116,** 525–560.

Kuo, H. L., 1973: Dynamics of quasi-geostrophic flows and instability theory. *Adv. Appl. Mech.,* **13,** 247–330.

Laprise, R., 1992: The resolution of global spectral models. *Bull. Amer. Meteor. Soc.,* **73,** 1453–1454.

Li, X., and B. Wang, 1994: Barotropic dynamics of the beta gyres and beta drift. *J. Atmos. Sci.,* **51,** 746–756.

Liebmann, B., H. H. Hendon, and J. D. Glick, 1994: The relationship between tropical cyclones of the western Pacific and Indian Oceans and the Madden–Julian oscillation. *J. Meteor. Soc. Japan,* **72,** 401–411.

Mak, M., and M. Cai, 1989: Local barotropic instability. *J. Atmos. Sci.,* **46,** 3289–3311.

Mapes, B., and R. A. Houze, 1992: An integrated view of the 1987 Australian monsoon and its mesoscale convective systems. I: Horizontal structure. *Quart. J. Roy. Meteor. Soc.,* **118,** 927–963.

McIntyre, M. E., and W. A. Norton, 1990: Dissipative wave–mean interactions and the transport of vorticity or potential vorticity. *J. Fluid Mech.,* **212,** 403–435.

Melander, M. V., J. C. Williams, and N. J. Zabusky, 1987: Axisymmetrization and vorticity-gradient intensification of an isolated

two-dimensional cyclone through filamentation. *J. Fluid Mech.*, **178,** 137–159.

Merrill, R. T., 1984: A comparison of large and small tropical cyclones. *Mon. Wea. Rev.*, **112,** 1408–1418.

Molinari, J., D. Knight, M. Dickinson, D. Vollaro, and S. Skubis, 1997: Potential vorticity, easterly waves and eastern Pacific tropical cyclogenesis. *Mon. Wea. Rev.*, in press.

Nitta, T., and M. Yanai, 1969: A note on the barotropic instability of the tropical easterly current. *J. Meteor. Soc. Japan,* **47,** 127–130.

——, and Y. Takayabu, 1985: Global analysis of the lower tropospheric disturbances in the tropics during the northern summer of the FGGE year. Part II: Regional characteristics of the disturbances. *Pure Appl. Geophys.*, **123,** 272–292.

——, Y. Nagakomi, Y. Suzuki, N. Hasegawa, and A. Kadokura, 1985: Global analysis of the lower-tropospheric disturbances in the tropics during the northern summer of the FGGE year. Part I: Global features of the disturbances. *J. Meteor. Soc. Japan,* **63,** 1–19.

Norquist, D. C., E. E. Recker, and R. J. Reed, 1977: The energetics of African wave disturbances as observed during phase III of GATE. *Mon. Wea. Rev.*, **105,** 334–342.

Numaguti, A., R. Oki, K. Nakamura, K. Tsuboki, N. Misawa, T. Asai, and Y.-M. Kodama, 1995: 4–5-day-period variation and low-level dry air observed in the equatorial western Pacific during the TOGA COARE IOP. *J. Meteor. Soc. Japan,* **73,** 267–290.

Peng, M. S., and R. T. Williams, 1986: Spatial instability of the barotropic jet with slow streamwise variation. *J. Atmos. Sci.,* **43,** 2430–2442.

Rayleigh, J. W. S., 1945: *The Theory of Sound.* Vol. 2. Dover, 504 pp.

Reed, R. J., and E. E. Recker, 1971: Structure and properties of synoptic-scale wave disturbances in the equatorial western Pacific. *J. Atmos. Sci.,* **28,** 1117–1133.

——, D. C. Norquist, and E. E. Recker, 1977: The structure and properties of African wave disturbances as observed during phase III of GATE. *Mon. Wea. Rev.*, **105,** 317–333.

Riehl, H., 1945: Waves in the easterlies and the polar front in the tropics. University of Chicago Department of Meteorology Misc. Rep. 17, 79 pp. [Available from Department of Meteorology, University of Chicago, 5734 S. Ellis Ave., Chicago, Ill 60637.]

Ripa, P., 1983: General stability conditions for zonal flows in a one-layer model on the β-plane or the sphere. *J. Fluid Mech.,* **126,** 463–489.

Saha, K., F. Sanders, and J. Schukla, 1981: Westward propagating predecessors of monsoon depressions. *Mon. Wea. Rev.,* **109**, 330–343.

Schubert, W. H., P. E. Ciesielski, D. E. Stevens, and H.-C. Kuo, 1991: Potential vorticity modeling of the ITCZ and the Hadley circulation. *J. Atmos. Sci.,* **48,** 1493–1509.

Shapiro, L. J., and K. V. Ooyama, 1990: Barotropic vortex evolution on a beta plane. *J. Atmos. Sci.,* **47,** 170–187.

Stevens, D. E., 1983: On symmetric stability and instability of zonal mean flows near the equator. *J. Atmos. Sci.,* **40,** 882–893.

Tai, K. S., and Y. Ogura, 1987: An observational study of easterly waves over the eastern Pacific in the northern summer using FGGE data. *J. Atmos. Sci.,* **44,** 339–361.

Takayabu, Y. N., and T. Nitta, 1993: 3–5 day-period disturbances coupled with convection over the tropical Pacific Ocean. *J. Meteor. Soc. Japan,* **71,** 221–246.

Thompson, O. E., and J. Miller, 1976: Hurricane Carmen: August–September 1974—Development of a wave in the ITCZ. *Mon. Wea. Rev.*, **104,** 1194–1199.

Thompson, R. M., S. W. Payne, E. E. Recker, and R. J. Reed, 1979: Structure and properties of the synoptic-scale wave disturbances in the intertropical convergence zone of the eastern Atlantic. *J. Atmos. Sci.,* **36,** 53–72.

Thorncroft, C. D., and B. J. Hoskins, 1994a: An idealized study of African easterly waves. I: A linear view. *Quart. J. Roy. Meteor. Soc.*, **120,** 953–982.

——, and ——, 1994b: An idealized study of African easterly waves. II: A nonlinear view. *Quart. J. Roy. Meteor. Soc.,* **120,** 983–1015.

——, ——, and M. E. McIntyre, 1993: Two paradigms of baroclinic-wave life-cycle behaviour. *Quart. J. Roy. Meteor. Soc.*, **119,** 17–55.

Tupaz, J. B., R. T. Williams, and C.-P. Chang, 1978: A numerical study of barotropic instability in a zonally varying easterly jet. *J. Atmos. Sci.,* **35,** 1265–1280.

Waliser, D. E., and C. Gautier, 1993: A global climatology of the ITCZ. *J. Climate,* **6,** 2162–2174.

Williams, R. T., H. Lim, and C.-P. Chang, 1984: Nonlinear and linear effects in an easterly jet with downstream variation. *J. Atmos. Sci.*, **41,** 621–636.

Yanai, M., 1961: A detailed analysis of typhoon formation. *J. Meteor. Soc. Japan,* **39,** 187–213.

Zehnder, J. A., 1991: The interaction of planetary-scale tropical easterly waves with topography: A mechanism for the initiation of tropical cyclones. *J. Atmos. Sci.,* **48,** 1217–1230.

Zehr, R. M., 1993: Recognition of mesoscale vortex initiation as stage one of tropical cyclogenesis. Preprints, *20th Conf. on Hurricanes and Tropical Meteorology,* San Antonio, TX, Amer. Meteor. Soc., 405–408.

Zhong, W., R. L. Gall, and J. A. Zehnder, 1993: Interannual variability of tropospheric waves in the tropics: A possible link with tropical cyclogenesis. *J. Atmos. Sci.,* **50,** 333–341.